Numerical Computation of Wishart Eigenvalue Distributions for Multistatic Radar Detection

by

Scott Jones

A Dissertation Presented in Partial Fulfillment
of the Requirements for the Degree
Doctor of Philosophy

Approved July 2019 by the
Graduate Supervisory Committee:

Douglas Cochran, Chair
Visar Berisha
Daniel Bliss
Oliver Kosut
Christ Richmond

ARIZONA STATE UNIVERSITY

August 2019

ABSTRACT

Eigenvalues of the Gram matrix formed from received data frequently appear in sufficient detection statistics for multi-channel detection with Generalized Likelihood Ratio (GLRT) and Bayesian tests. In a frequently presented model for passive radar, in which the null hypothesis is that the channels are independent and contain only complex white Gaussian noise and the alternative hypothesis is that the channels contain a common rank-one signal in the mean, the GLRT statistic is the largest eigenvalue λ_1 of the Gram matrix formed from data. This Gram matrix has a Wishart distribution. Although exact expressions for the distribution of λ_1 are known under both hypotheses, numerically calculating values of these distribution functions presents difficulties in cases where the dimension of the data vectors is large. This dissertation presents tractable methods for computing the distribution of λ_1 under both the null and alternative hypotheses through a technique of expanding known expressions for the distribution of λ_1 as inner products of orthogonal polynomials. These newly presented expressions for the distribution allow for computation of detection thresholds and receiver operating characteristic curves to arbitrary precision in floating point arithmetic. This represents a significant advancement over the state of the art in a problem that could previously only be addressed by Monte Carlo methods.

ACKNOWLEDGMENTS

A great many mentors, advisors, colleagues, family, and friends deserve mention in contributions both technical and otherwise to this dissertation. First and foremost, I feel extremely fortunate to have had the opportunity to work with and learn from my advisor Douglas Cochran. His knowledge of signal processing and mathematics and attention to detail while approaching challenging problems has had an enormous impact on the way I approach engineering and mathematics. It has also resulted in learning many unexpected things about motorcycles, cooking, and T.V. and cinema from before I was born.

Many others at ASU that have had an impact on my formative development as an engineer and researcher. Thank you to the members of my thesis committee - Visar Berisha, Daniel Bliss, Oliver Kosut, and Christ Richmond. I am grateful for both the ways they have helped me learn technically through coursework and research discussions and for their excellent professional and personal advice. Many thanks to my fellow graduate students for providing an engaging environment in which to grow as an engineer. In particular, I must extend my gratitude to Lauren Crider for the hours of critique in front of a whiteboard and being a great friend throughout our studies.

There are many people outside of ASU from whom I am grateful to have had the opportunity to learn and have been influential in my academic and professional development. Most importantly, thank you to Vaughan Clarkson, formerly at the University of Queensland, Brisbane, Australia and to Stephen Howard of Defence Science and Technology Group Australia for being particularly influential in their guidance and mentoring throughout this project and their strong impact on the direction of my graduate education.

Thank you to everyone outside of academia that has provided support throughout

my time at ASU. I am extremely grateful for my parents Marilyn and Gary and my sister Erin, and I cannot thank them enough for a lifetime of support and encouragement in all my professional and personal pursuits. Dillon, Drew, Ryan, Quintana, Sarah, Jonathan, Jason, Aaron, Kari, and the many other friends I have been so fortunate to have surrounding me during my time at ASU – thank you for being a constant source of balance and a reminder that there is a life outside of engineering.

This work was supported in part by the U.S. Air Force Office of Scientific Research under Grant Nos. FA9550-18-1-0190 and FA9550-12-1-0225 and in part by the U.S. National Science Foundation under EAPSI Grant No. 1614403.

TABLE OF CONTENTS

CHAPTER Page

CHAPTER Page

LIST OF TABLES

LIST OF FIGURES

Figure Page

Figure Page

Chapter 1

INTRODUCTION

Recent research directions in multi-sensor statistical signal processing (e.g., [5, 6, 7, 8, 9, 10]) and MIMO communications (e.g., [1, 11, 12, 13]) have brought significant attention to the roles of complex Wishart matrices in these application areas. Wishart matrices have a long history in the statistical literature [14, 15, 16]; they arise naturally in multi-channel sensing and MIMO applications when the received data is modeled as being complex normally distributed. In particular, statistics used for detection, estimation, and characterization of collected data are often functions of the Gram matrix formed from the received data, which is a complex Wishart matrix under typical Gaussian data models.

This dissertation examines a problem motivated by multi-channel detection, as arises in multistatic passive radar, where it is to be ascertained whether a common signal is present across several noisy channels. In some such problems, a subset of the channels may be "reference channels" known to contain a noisy copy of the common signal of interest, or all channels may be "surveillance channels" which may or may not contain the common signal. The surveillance-only scenario is the primary motivation for the analysis in this dissertation, and is discussed in [2, 17], though the results apply to a broader class of detection problems [18, 19].

The largest eigenvalue of the $M \times M$ Gram matrix formed from the complex data was shown in [20] to be a sufficient statistic for the Generalized Likelihood Ratio Test (GLRT) for a rank-one signal in M channels of independent zero-mean white Gaussian noise (ZMWGN). Typical multi-receiver detection scenarios involve a relatively small number of sensors (generally $M < 10$), but detection of weak signals

may require the length N of data sequences collected at each sensor to be on the order of $10^5 - 10^6$ or larger. To set detection thresholds corresponding to desired false alarm probabilities in such situations, it is thus necessary to compute the distribution of λ_1 under the null hypothesis for small values of M and very large values of N; complete performance analysis of the detectors requires computation of the distribution under the alternative hypothesis as well.

At this point, it is important to emphasize that the distribution of λ_1 is known from classical statistical results in the null hypothesis case [15] and from more recent work in MIMO communications under the alternative hypothesis [21]. The issue addressed in this dissertation is that these formulations of the distributions are not amenable to numerical evaluation except for relatively small values of M and N. Commonly-used approximation or asymptotic methods, such as those involving the Tracy-Widom distribution [22], lack sufficient fidelity for the desired ranges of M and N and may not be sufficiently accurate in the tail of the distribution, which is of the greatest interest in multi-channel sensing applications in which low false-alarm operating regimes are the norm. Monte Carlo methods, including those that incorporate variance reduction methods such as importance sampling [23, 24], have been used to analyze these distributions. However, they are not computationally viable in the low false-alarm regimes entailed in radar surveillance applications for a variety of reasons. These methods are generally problem specific (e.g., taking the limit in both N and M at some fixed ratio; in this problem M is generally small), are very non-trivial to derive and construct, and are designed only for the central distribution. In the regimes of interest for multi-channel detection problems, which often require very low false-alarm probabilities, these methods generally provide only modest performance gains that are insufficient for setting detection thresholds.

This thesis presents methods to compute the distribution of λ_1 under the null

hypothesis in which the M channels contain independent ZMWGN, referred to in the literature as a "central" Wishart distribution, and the alternative hypothesis under which a common signal is present in the mean across each channel, which is referred to as a "non-central" Wishart distribution. In addition these methods are extended to the distribution of λ_1 in the case of a non-identity covariance matrix, which is not of direct interest to the detection problem presented but has applications in MIMO communications [21]. The results for the central distribution allow for closed form computation of detection thresholds; when combined with the results for the non-central distribution it is possible to compute receiver operating characteristic (ROC) curves to arbitrary precision in the low-false alarm regimes of interest for multistatic passive radar applications. Chapter 2 presents a model for the multistatic detection problem derived from physical phenomenology, derives detection statistics, and presents classical results on probability distributions on these statistics and their numerical shortcomings. First, Section 2.1 presents the physical model of the passive radar scenario that motivates this work and gives rise to the model for the data. Section 2.2 derives GLRT statistics for the binary decision problem presented by the signal model. Section 2.4 discusses classical and modern results on the distributions of the largest eigenvalue of Wishart matrices. The intractability of these results for this class of detection problem is demonstrated in 2.5. Chapter 3 contains the primary theoretical contributions of this thesis, in which the classical distributions for λ_1 are expanded as inner products of Laguerre polynomials, which allows for tractable computation of probabilities through quadrature integration. The particular cases of the central, non-central, and central correlated distributions are treated in Sections 3.1, 3.2, and 3.3, respectively. Results from numerical experiments are presented in Chapter 4, which includes comparison of CDF computation to Monte Carlo methods, computing detection thresholds, and computing ROC curves. Specific contributions

of this thesis and possible future directions for this research and applications to related problems are discussed in Chapter 5.

Chapter 2

MULTISTATIC PASSIVE RADAR AND EXISTING RESULTS

This chapter presents a formulation of the multistatic passive radar detection problem that is the primary motivation of the work, along with existing results on detection statistics and probability distributions on these statistics as derived in classical random matrix theory. Section 2.1 presents a model for the data collected at each geographically distributed radar receiver resultant from RF propagation and the physical geometry of the problem. The initial signal processing performed on the data to time align and undo Doppler shifts induced by the putative physical state of the target whose presence is to be ascertained is also discussed. Next, Section 2.2 presents a derivation of the generalized likelihood ratio test (GLRT) statistic for the binary hypothesis problem presented in the preceding section, as originally seen in [20]. The Bayesian detection statistic for the same binary hypothesis problem is also presented. Classical random matrix theory results for the largest eigenvalue distribution in the central Wishart case as originally derived in [15] are seen in Section 2.4. This section also discusses more modern generalizations of these results to the non-central and central correlated cases. This chapter then concludes in Section 2.5 with a discussion of the numerical limitations of these classical results and thus the reasons they are not suitable for computing probabilities in the presented formulation of the multistatic passive radar detection problem, and some discussion of previous

efforts to find a numerically tractable formula for the distribution.

2.1 Signal Model

This section presents a signal model for detection in multistatic passive radar, beginning with a physical model for the data recorded at each receiver. Section 2.2 uses this to formulate a binary hypothesis problem, gives an overview of the derivation of GLRT and Bayesian statistics for the rank-K detection problem, and discusses the rank-1 scenario that is the subject of analysis for the remainder of the dissertation.

This dissertation considers the passive radar scenario described in [2]. The presence or absence of a target with a given isolated state (position and velocity) is to be deduced from sensor data. The target may be itself transmitting RF energy or be a scatterer reflecting energy from some illuminator or illuminators in the environment. In the case that the target is a scatterer, as in [2] it is assumed that the transmitted signal only manifests in the data through scattering off the target; i.e., no direct-path signal appears in the sensor data, and there is no clutter. In practice, this situation would occur if physical obstacles prevent direct-path propagation of the transmitted signal to the receivers. The positions of M receivers, and in the case that the target is a scatterer, the transmitter, are assumed known and fixed. Although motivated by this scenario, the results presented below are more broadly applicable in multi-channel detection.

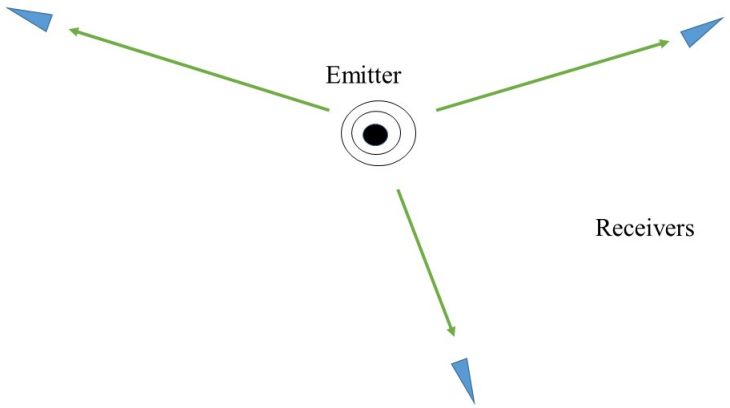

Figure 2.1: Signal Model Geometry.

In addition to a scalar gain and additive Gaussian noise, each channel imparts time delay and Doppler to the transmitted signal in accordance with the putative target state and the corresponding sensor position. The analog signal at each receiver is filtered at each receiver and sampled to convert to a digital time series. Delay and Doppler are compensated at each receiver ultimately yielding M complex data vectors, each of length N, which are tested for common signal content. It is assumed the signal of interest is narrow band, allowing for the following approximations to be used.

If a target is present at position $\mathbf{p}$ moving at velocity $\mathbf{v}$, the signal at each receiver will depend on two parameters, the time delay τ_m and the frequency shift ω_m. The time delay is calculated as the time the signal takes to propagate from the transmitter located at position $\mathbf{t}$ to the m^{th} receiver located at position $\mathbf{r}_m$ via the target, and is calculated as

$$\tau_m = \frac{1}{c}\left(\|\mathbf{p}-\mathbf{t}\| + \|\mathbf{p}-\mathbf{r_m}\|\right). \tag{2.1}$$

where c is the speed of light. Note of course if the target is itself the transmitter, $\mathbf{p} = \mathbf{t}$. The frequency shift corresponding to the target traveling at a particular

velocity is given by the standard approximation

$$\omega_m = \frac{\omega_0}{c}\left(\left\|\frac{(\mathbf{p}-\mathbf{t})(\mathbf{p}-\mathbf{t})^\dagger}{\|\mathbf{p}-\mathbf{t}\|^2}\mathbf{v}\right\| + \left\|\frac{(\mathbf{p}-\mathbf{r_m})(\mathbf{p}-\mathbf{r_m})^\dagger}{\|\mathbf{p}-\mathbf{r_m}\|^2}\mathbf{v}\right\|\right) \tag{2.2}$$

ω_0 is the center frequency of the transmitted signal s. The signal at the m^{th} receiver is thus

$$x_m(t) = \eta_m s(t-\tau_m)e^{i\omega_m t} + \nu_m(t) \tag{2.3}$$

where η_m is the signal amplitude and $\nu_m(t)$ is receiver noise.

To test for the presence of a target postulated to be at a particular position and traveling at a particular velocity, the data is corrected using the postulated frequency shift and time delay to form the vectors

$$\tilde{x}_m(t) = \eta_m x_m(t+\tau_m)e^{-i\omega t} = \mu_m x(t) + \nu_m(t). \tag{2.4}$$

$\xi_m(t)$ is the modified noise component. Note that $\nu_m(t)$ is assumed to be additive zero-mean white Gaussian noise, independent and identically distributed at each receiver.

Following sampling at an appropriate (Nyquist) rate, the analog signal at each receiver is digitized as a length N vector. Under the null hypothesis $\mathcal{H}_0$ that the received data contain only noise, these vectors $\tilde{x}_m$, $m = 1, \ldots, M$ are given by

$$\mathcal{H}_0 : \tilde{x}_m = \nu_m$$

where the ν_m are independent N-vectors of zero-mean complex Gaussian noise. Under the alternative hypothesis,

$$\mathcal{H}_1 : \tilde{x}_m = \eta_m s + \nu_m$$

where η_m is a complex channel gain and s is a unit modulus complex N-vector representing the common signal component across all M channels. Throughout the dissertation, these vectors will be considered as columns of the matrix X, i.e.

$$X = [\tilde{x}_1, \ldots, \tilde{x}_M].$$

2.2 Maximum-Likelihood Parameter Estimation

The GLRT statistic for the problem of interest is first derived as a generalized linear model as described in [20], for the general case of a rank K signal present across M receivers. The case of particular interest for this dissertation, that of the distribution of this statistic for a rank 1 signal across M channels, is subsequently discussed as a special case.

The signal model described in Section 2.1 is a specific case of the more general linear model described in [20]. The data is modeled as a matrix $X \in \mathbb{C}^{N\times M}$ with elements representing the data at the m^{th} sensor at time instant n, where

$$X = SA + \nu$$

Where ν is additive complex white Gaussian noise with variance σ^2, $S \in \mathbb{C}^{N\times K}$ is an unknown matrix describing the signal subspace. The matrix $A \in \mathbb{C}^{K\times M}$ contains unknown complex amplitudes of channel gains between the k^{th} signal subspace component and the m^{th} receiver. Thus, the detection problem becomes

$$\mathcal{H}_0 : X \sim \mathcal{CN}(0, \sigma^2 I)$$
$$\mathcal{H}_1 : X \sim \mathcal{CN}(SA, \sigma^2 I).$$

The probability density function of X under $\mathcal{H}_0$ condition on σ^2 is

$$p(X|\mathcal{H}_0, \sigma^2) = \frac{1}{(\pi\sigma^2)^{-MN}} e^{-\frac{1}{\sigma^2}\mathrm{Tr}(X^\dagger X)}$$

While under $\mathcal{H}_1$, the probability density function conditioned on σ^2, A, and S is

$$p(X|\mathcal{H}_1, \sigma^2, A, S) = \frac{1}{(\pi\sigma^2)^{MN}} e^{-\frac{1}{\sigma^2}\mathrm{Tr}\left((X-AS)^\dagger(X-AS)\right)}.$$

The generalized likelihood ratio test is then calculated as the ratio of these PDFs. In this dissertation, it will be assumed the noise variance is known; the case estimating

an unknown noise variance is readily computed using similar techniques and can be seen in [20]. The GLRT is

$$L(X) = \frac{\max_{A,S} p(X|A,S,\sigma^2)}{p(X|\sigma^2)} \gtrless_{\mathcal{H}_0}^{\mathcal{H}_1} \gamma.$$

The ML estimate for the amplitude matrix is $\hat{A} = XS^\dagger$. To estimate S, the Schur-Horn theorem is used to maximize over $P = S^\dagger S$ yielding $\hat{P} = \sum_{k=1}^{K} v_k v_k^\dagger$ where v_k are the unit norm eigenvalues of $W = X^\dagger X$ [25].

$$\begin{aligned} L(X) &= e^{\frac{1}{\sigma^2}\mathrm{Tr}(XS^\dagger SX^\dagger)} \\ &= e^{\frac{N}{\sigma^2}\mathrm{Tr}(WP)} \\ &= e^{\frac{N}{\sigma^2}\sum_{i=1}^{k}\lambda_i} \end{aligned}$$

where $\lambda_1 \geq \ldots \lambda_M \geq 0$ are the ordered, non-negative eigenvalues of $X^\dagger X$. Taking the logarithm and absorbing known constants, the statistic becomes

$$\ell(X) = \sum_{i=1}^{K} \lambda_i. \tag{2.5}$$

Note that in the case that σ^2 is unknown, the statistic is

$$\ell(X) = \left(1 - \frac{\mathrm{Tr}(DP)}{\mathrm{Tr}(D)}\right)^{-MN}$$

where $D = \mathrm{diag}(\lambda_1, \ldots, \lambda_n)$. A proof is shown in [20]. This statistic can also be written, perhaps more intuitively, as a function of the eigenvalues as

$$\ell(X) = \left(1 - \frac{\sum_{i=1}^{K}\lambda_i}{\sum_{i=1}^{N}\lambda_i}\right)^{-MN}. \tag{2.6}$$

In the Bayesian approach, the parameters A, S, and σ^2 may be marginalized out of the likelihood functions in which it appears by integration with respect to a non-informative prior. In the case of known noise variance, the likelihood ratio is

$$\ell(X) = Qe^{\frac{N\alpha}{\sigma^2}\sum_{i=1}^{K}\lambda_i}\Pi_{i=1}^{N-K}\Pi_{j=1}^{K}\frac{1}{\lambda_j - \lambda_{K+i} + \frac{\sigma^2}{\alpha}}$$

where Q is a function of the volume of the Grassmannian consisting of K-dimensional subspaces of N dimensional space. A similar result is found for the case of unknown noise variance; a full derivation may be seen in [20].

The physical model described in Section 2.1 contains parameters for the delay and Doppler, of the signal across each of M channels. By postulating a target position and velocity, and performing corrections as shown in 2.1, (2.5) can be applied to data arising from physical phenomenology corresponding to the signal model (2.3). In the case of interest in this dissertation, a target of rank $K = 1$ will be considered, so the GLRT reduces to

$$\ell(X) = \lambda_1$$

The remainder of this dissertation will examine the probability distribution of λ_1 under the $\mathcal{H}_0$ case, with an aim of analytically computing thresholds as a function of the probability of false alarm for a passive radar operating as a multi-channel detector. The probability distribution will be derived using known techniques, and some limitations of these known results as applicable to the problem of interest will be discussed. New results will be presented that overcome these numerical limitations, and allow for thresholds to be set analytically in this problem.

2.3 Defining SNR

It is assumed throughout this dissertation that the white Gaussian noise across each receiver channel it known to have equal and unit variance. The SNR across each channel is entirely dependent on the complex channel gain parameter η_m seen in Section 2.1 in the expressions for the alternative hypothesis. The behavior of the distribution under the alternative hypothesis is dependent only on the largest and only non-zero eigenvalue of the Gram matrix formed by the rank-one matrix in the mean of the signal model. Therefore, it is possible to achieve the same performance

with differing SNR levels across each of the channels. However, in latter parts of this dissertation, in particular in numerical examples seen in Chapter 4, SNR is generally referred to by channel for purposes of intuition and to facilitate a description in units of decibels, and in simulations is generally assumed to equal across each channel. The relationship between the complex channel gains η_m defining the SNR and the parameter μ_1, the largest eigenvalue of the mean Grammian of the distribution of the statistic under $\mathcal{H}_1$ is given by N times the norm of the vector of the weights of the signal on each individual channel.

$$\mu_1 = N \left\| (\eta_1, \ldots, \eta_M) \right\|^2 \tag{2.7}$$

2.4 Derivation of Classical Distributions

This section presents formulas for the distribution of λ_1 as first seen in classical statistical literature for the central case, which has been generalized to the non-central case in more recent MIMO communications literature. These formulas will be the starting point for closed form analysis, but it will be clear that they do not allow for numerical computation of probabilities in scenarios of interest for multistatic passive radar.

2.4.1 The Central Distribution

The form of the distribution of the largest eigenvalue of a complex central Wishart matrix most commonly seen in the literature follows from a derivation in Khatri's paper [15]. This section follows Khatri's derivation of the CDF from the joint PDF of the ordered eigenvalues, but in keeping consistent with previous sections, the notation from Tulino and Verdú's book is used [11]. The joint PDF of the ordered eigenvalues is

$$f(\lambda_1, \ldots, \lambda_M) = e^{-\sum_{i=1}^{M} \lambda_i} \prod_{i=1}^{M} \frac{\lambda_i^{N-M}}{(N-i)!(M-i)!} \prod_{j=1}^{M-1} \prod_{k=j+1}^{M} (\lambda_j - \lambda_k)^2. \tag{2.8}$$

Two lemmas from Khatri are necesssary to derive this form of the CDF [15]. The first concerns the separability of the integral - how summing over permutations of exponents allows the domain of the integral of interest to be changed from a simplex to a box.

Lemma 1 *Suppose* $\mathcal{D} = \{0 \leq x_M \leq \ldots \leq x_1 \leq x\}$, *and let* (M_{t_j}, N_{t_j}) *be any permutation of* $(M_k, N_k), \ldots, (M_1, N_1)$, *and consider summation taken over all such permutations. Then*

$$\sum \int_{\mathcal{D}} \prod_{j=1}^{k} \left(x_j^{M_{t_j}} (1 - x_j)^{N_{t_j}} dx_j \right) = \prod_{j=1}^{k} \left(\int_0^x x_j^{M_j} (1 - x_j)^{N_j} dx_j \right) \tag{2.9}$$

Note that this lemma is derived for the case of normalized eigenvalues; the $(1-x)^n$ term becomes an exponential for large n. The second lemma concerns the determinant of a particular matrix

Lemma 2 *Let* $\sum$ *mean summation over all permutations* $j_1, j_2, \ldots, j_m$ *of* $1, 2, \ldots, M$.

$$\prod_{j=1}^{M-1} \prod_{k=j+1}^{M} (x_j - x_k)^2 = \sum \begin{vmatrix} x_{j_1}^{2M-2} & x_{j_2}^{2M-3} & \cdots & x_{j_M}^{M-1} \\ x_{j_1}^{2M-3} & x_{j_2}^{2M-4} & \cdots & x_{j_M}^{M-2} \\ \vdots & \vdots & \ddots & \vdots \\ x_{j_1}^{M-1} & x_{j_2}^{M-2} & \cdots & x_{j_M}^{0} \end{vmatrix} \tag{2.10}$$

This follows from squaring the known form of a Vandermonde determinant.

Using the two lemmas, it is possible to integrate (2.8) to marginalize the $M-1$ smallest eigenvalues and thus obtain the CDF of the largest eigenvalue λ_1.

Theorem 1 *The CDF of the largest eigenvalue λ_1 of W is*

$$F_{\lambda_1}(x) = \frac{|\gamma(N+i+j,x)|_{i,j=0,\ldots,M-1}}{\prod_{k=1}^{M}\Gamma(N-k)\Gamma(M-k)}$$

where γ is the lower incomplete gamma function and Γ is the complete gamma function.

Compute the CDF by integrating the PDF given in the first section

$$F_{\lambda_1}(x) = \int_{\mathcal{D}} f(\lambda_1,\ldots,\lambda_M)d\lambda_1\cdots d\lambda_M$$

where $\mathcal{D} = \{0 \le x_M \le \ldots \le x_1 \le x\}$. First, using Lemma 2 and factoring the exponential term into the product results in

$$F_{\lambda_1}(x) = \sum \int_{\mathcal{D}} \begin{vmatrix} \lambda_{j_1}^{2M-2} & \lambda_{j_2}^{2M-3} & \cdots & \lambda_{j_M}^{M-1} \\ \lambda_{j_1}^{2M-3} & x_{j_2}^{2M-4} & \cdots & \lambda_{j_M}^{M-2} \\ \vdots & \vdots & \ddots & \vdots \\ \lambda_{j_1}^{M-1} & \lambda_{j_2}^{M-2} & \cdots & \lambda_{j_M}^{0} \end{vmatrix} \prod_{i=1}^{M} \frac{e^{-\lambda_i}\lambda_i^{N-M}}{(N-i)!(M-i)!} d\lambda_1\cdots d\lambda_M. \tag{2.11}$$

The determinant in the integrand can be written as

$$\sum \operatorname{sgn}(t_1,\ldots,t_M)\lambda_{j_1}^{M-1+t_1}\lambda_{j_2}^{M-2+t_2}\cdots\lambda_{j_M}^{t_M}$$

where $t_1,\ldots,t_M$ is a permutation of $0,1,\ldots,M-1$ and $\operatorname{sgn}(t_1,\ldots,t_M)$ is positive for an even permutation and negative for an odd permutation. Then the integral is equivalent to

$$\begin{aligned} F_{\lambda_1}(x) = \sum_t \sum_j \int_{\mathcal{D}} \operatorname{sgn}(t_1,\ldots,t_M)\lambda_{j_1}^{M-1+t_1}\lambda_{j_2}^{M-2+t_2}\cdots\lambda_{j_M}^{t_M} \\ \times \prod_{i=1}^{M} \frac{e^{-\lambda_i}\lambda_i^{N-M}}{(N-i)!(M-i)!} d\lambda_1\cdots d\lambda_M \end{aligned} \tag{2.12}$$

where the sums are over all permutations of t_i and j_i. Next, apply lemma 1 to change the domain of integration from $\mathcal{D}$ to the box $[0, x]^m$, eliminate one of the permutation sums, and factor the product.

$$F_{\lambda_1}(x) = \sum_t \operatorname{sgn}(t_1, \ldots, t_M) \prod_{i=1}^{M} \frac{1}{\Gamma(N-i)\Gamma(M-i)} \int_0^x \lambda_i^{N-i+t_j} e^{-\lambda_i} d\lambda_i \tag{2.13}$$

Factoring out the constant term and recognizing that the integrand is an incomplete gamma function, and the permutation summation is the Leibniz formula for a determinant, the CDF can be written as

$$F_{\lambda_1}(x) = \frac{|\gamma(N-M+i+j+1, x)|_{i,j=0,\ldots,M-1}}{\prod_{k=1}^{M} \Gamma(N-k)\Gamma(M-k)}. \tag{2.14}$$

As $F \to 1$ as $x \to \infty$, the normalizing constant must tend to the limit of the numerator, i.e. to a determinant of complete gamma functions. Therefore the CDF can be written

$$F_{\lambda_1}(x) = \frac{|\gamma(N-M+i+j+1, x)|_{i,j=0,\ldots,M-1}}{|\Gamma(N-M+i+j+1)|_{i,j=0,\ldots,M-1}}. \tag{2.15}$$

This form is of interest for numerical rehabilition. Note that the lemmas here can be generalized to derive expressions of a similar form for correlated central and uncorrelated non-central Wishart matrices, as discussed in the following section. For further detail, see [3].

2.4.2 The Non-Central and Correlated Distributions

Recent results motivated by MIMO communications generalize Khatri's result to the non-central case and the central correlated case. In particular, the following theorem is given in [21].

Theorem 2 *Given two arbitrary matrices $\Phi(x)$ and $\Psi(x)$ with ij^{th} elements $\Phi_i(x_j)$ and $\Psi_i(x_j)$ and an arbitrary function $\xi(x)$, the following identity holds:*

$$\int \cdots \int_{\mathcal{D}} |\Phi(\mathbf{x})| \cdot |\Psi(\mathbf{x})| \prod_{k=1}^{M} \xi(x_k) d\mathbf{x} = \left| \int_a^b \Phi_i(x) \Psi_j(x) \xi(x) dx \right|_{i,j=0,\ldots,M-1} \tag{2.16}$$

such that $\mathcal{D} = \{b \geq x_1 \geq \ldots \geq x_M \geq a\}$.

A proof of this result as well as similar theorems regarding integration over different domains $\mathcal{D}$ are given in [21]. This case is of particular interest as it allows Khatri's results to be generalized to the non-central and central correlated cases. The joint PDFs of the ordered eigenvalues of a complex Wishart matrix of each case can be written with functions ξ and matrices with a Vandermonde-like structure, allowing application of the theorem. A table of the appropriate choices for ξ, Ψ, Φ can be seen in [3].

First, consider the case of the non-central CDF of λ_1 with an arbitrary rank K mean.

$$F_{\lambda_1}(x) = \frac{1}{C} \left| \begin{cases} \int_0^x {}_0F_1(N-M+1, \mu_j t) t^{N-i+1} e^{-t} dt, \\ \qquad j = 0, \ldots, K-1, i = 0, \ldots, M-1 \\ \int_0^x t^{N-M+i+j+1} e^{-t} dt, \\ \qquad j = K, \ldots, M, i = 0, \ldots, M-1 \end{cases} \right|. \tag{2.17}$$

In this expression, C is a normalizing constant equal to the limit of the determinant term as $x \to \infty$, and μ_i

Second, for completion, Chiani et al.'s work presents the CDF of λ_1 under with an arbitrary covariance matrix. In most commonly presented detection problems in the literature involving a correlated central Wishart distribution generally, λ_1 is generally not a sufficient statistic; rather an expression involving all M eigenvalues is often required [20]. Nevertheless, this distribution has more than just academic

interest, as it arises in MIMO channel models with either transmit or receive side correlation [21]. The CDF of λ_1 in this case is given by

$$F_{\lambda_1}(x) = \frac{1}{C} \left| \sigma_j^{N-M+i+1} \int_0^{x/\sigma_j} t^{N-M+i+2} e^{-t} dt \right|_{i,j=0\ldots M-1} . \tag{2.18}$$

2.5 Numerical Issues

Considering $\mathcal{H}_0$, suppose X is an $M \times N$ matrix with independent identically distributed complex normal entries having mean zero and unit variance; i.e., $x_{ij} \sim \mathcal{CN}(0,1)$. The Gram matrix $G = XX^\dagger$ generated from this data has a central complex Wishart distribution $G \sim \mathcal{CW}(N, I_M)$. As noted above, the GLRT for detection of a rank-one signal in this setting is based on the largest eigenvalue λ_1 of this Gram matrix, and hence establishing thresholds for constant false-alarm rate detection requires explicit evaluation of the CDF of this eigenvalue. The CDF of λ_1, as given in [1], is

$$F_{\lambda_1}(x) = \frac{|\gamma(N-M+i+j+1, x)|_{i,j=0,\ldots,M-1}}{|\Gamma(N-M+i+j+1)|_{i,j=0,\ldots,M-1}} \tag{2.19}$$

where $\gamma(a,x) = \int_0^x t^{a-1} e^{-t} dt$ is the lower incomplete gamma function.

The form of the CDF F_{λ_1} presented in (2.15) strongly constrains the problem size for which explicit calculations are possible using floating point arithmetic. Direct computation using a naive implementation of this expression, while exact in principle, is severely limited by the maximum number of samples possible before overflowing double precision floating point.

Sensors (M)	Maximum Samples (N)
2	98
3	71
4	57
5	47

Table 2.1: Computational Limits of Expression from [1] in Double Precision Floating Point Arithmetic.

Realistic problems for passive radar applications require numbers of samples N on the order of $10^5 - 10^6$, generally with a single-digit number of receivers. The previous best implementation, given in [2], allowed for computation in problems of this size only for two or three receivers in the $\mathcal{H}_0$ case.

Sensors (M)	Maximum Samples (N)
2	4.8×10^8
3	2.6×10^5
4	4.5×10^3
5	5.5×10^2

Table 2.2: Computational Limits of Expression from [2] in Double Precision Floating Point Arithmetic.

The floating point overflow limits in the $\mathcal{H}_1$ case are similar to those seen in Table 2.1 in the rank one case. Columns $2, \ldots, M$ contain incomplete gamma function entries identical to the $\mathcal{H}_0$ case, while the first column contains an integral with an integrand containing terms equivalent to a lower order gamma function multiplied by a hypergeometric function.

Sensors (M)	Maximum Samples (N)
2	101
3	75
4	57
5	47

Table 2.3: Computational Limits of Expression from [3] in Double Precision Floating Point Arithmetic.

The point at which overflow occurs may shift by one to two samples dependent on the magnitude of the eigenvalue of the mean Gramian; regardless these numbers are on the same order of magnitude as the $\mathcal{H}_0$ case and are insufficient for multistatic passive radar problems where the number of samples required could be on the order of 10^6 or greater.

Chapter 3

LAGUERRE POLYNOMIAL EXPANSION

This chapter represents the primary theoretical contribution of this dissertation. The classical expressions for the distributions of the largest eigenvalue λ_1 of a complex Wishart matrix seen in Section 2.4 were shown in Section 2.5 to overflow double precision arithmetic in cases of interest for the multistatic passive radar detection problem described in Section 2.1 and 2.2. This section focuses on the relationship between the gamma function and the generalized Laguerre family of orthogonal polynomials, and makes use of this relationship to rewrite the classically known expressions for these distributions as inner products of polynomials. Through some further manipulation, these inner product expressions may be made amenable to high accurate computation of probabilities using double precision floating point arithmetic in regimes of interest, where the degrees of freedom N determined by the number of samples is large. Furthermore, these expressions may prove to be very practical for application to a multi-channel detection problem in which it is of interest to operate at a very low probability of false alarm. In this operating regime, the tail of the distribution is what is of primary interest for setting detection thresholds. Generating empirical estimates of the distribution through pseudo-random trials would be extremely time intensive to provide a sufficiently accurate approximation of the distribution.

This chapter is divided into three sections, corresponding to the three cases of complex Wishart matrix commonly examined in the literature. Section 3.1 derives an expression for the central case, corresponding to the $\mathcal{H}_0$ hypothesis in the proposed detection problem. Section 3.2 derives an expression for the non-central case corresponding to the $\mathcal{H}_1$ hypothesis. Finally, Section 3.3 derives an expression for the

correlated central case, which does not directly appear in the proposed multistatic detection problem, but has been examined in the literature as a quantity of interest in MIMO communications applications.

3.1 Derivation for the $\mathcal{H}_0$ Distribution

This section presents a derivation of a computationally tractable formula for the distribution of λ_1 under the $\mathcal{H}_0$ hypothesis as originally seen in [26]. First, the formula for the distribution as given by (2.15) is expanded as inner products of generalized Laguerre polynomials. The problematic terms, namely normalization constants that arise in the inner products and the gamma function integrand terms in the inner products, are dealt with through the use of a substitution and computation of terms in quickly convergent series. Finally, a new family of orthogonal polynomials is introduced that are orthogonal on the resultant integration range due to the change of variables, and a concise formula for the desired distribution in terms of inner products of these polynomials is presented.

3.1.1 Laguerre Polynomial Conjugation

In order to write $F_{\lambda_1}^{\mathcal{H}_0}$ in a form that can be computed using floating point arithmetic for practical problem sizes in multistatic passive radar applications, it is necessary to rewrite the distribution such that the intermediate terms in the determinant expression for the distribution can be computed without overflowing floating point representations. Begin with the distribution of λ_1 (2.15) under the $\mathcal{H}_0$ hypothesis as given by Khatri, that the data across each of the M sensors consists of independent zero-mean complex white Gaussian N vectors. Throughout this section and to differentiate from the other cases for the remainder of the dissertation, the CDF of λ_1 in the central case will be referred to using the notation $F_{\lambda_1}^{\mathcal{H}_0}$. Originally shown in

(2.15), the formula for the central CDF of λ_1 commonly seen in the literature is

$$F_{\lambda_1}^{\mathcal{H}_0}(x) = \frac{|\gamma(N-M+i+j+1,x)|_{i,j=0,\ldots,M-1}}{|\Gamma(N-M+i+j+1)|_{i,j=0,\ldots,M-1}}.$$

This formula for the distribution is numerically unwieldy due for large values of N encountered in multistatic passive radar applications due to the large gamma functions that must be computed as intermediate terms in computing probabilities. These will be eliminated via an expansion as inner products of orthogonal polynomials. Define $\Xi(x)$ to be the matrix in the numerator of this expression for the CDF containing gamma function entries, and let A be the lower triangular matrix of generalized Laguerre polynomials $L_i^{(a)}$ of degree $0\ldots,M-1$, such that $a = N-M$. Define the matrix Ψ as the conjugation of Ξ by A.

$$\Psi(x) = A^T \Xi(x) A$$

Then the distribution of λ_1 can be written

$$\begin{aligned} F_{\lambda_1}^{\mathcal{H}_0}(x) &= \frac{|\Xi(x)|}{|\Xi(\infty)|} \\ &= \frac{\left|A^T \Xi(x) A\right|}{|A^T \Xi(\infty) A|} \\ &= \frac{|\Psi(x)|}{|\Psi(\infty)|} \end{aligned}$$

where the individual elements of the matrix Ψ take the form

$$\Psi_{ij} = \sqrt{\frac{i!j!}{(a+i)!(a+j)!}} \int_0^x L_i^{(a)}(t) L_j^{(a)}(t) t^a e^{-t} dt \qquad i,j = 0,\ldots,M-1. \tag{3.1}$$

It is clear that as $x \to \infty$, (3.1) evaluates to δ_{ij} and therefore the denominator is the identity. Note that the elements of the matrix Ψ given by (3.1) are still numerically intractable after conjugation by the coefficients of the generalized Laguerre polynomials. This is due to the large leading constant of order approximately $N!$ on each

element, as well as the continued presence of the $t^a e^{-t} dt$ term, which is of course the integrand of a gamma function. To eliminate these extremely large numerical cancellations, it is proposed to change variables and thus the domain of integration in such a way that will allow cancellation of some of these terms in the expression prior to any computation being performed.

3.1.2 Computing the Matrix Elements

The individual elements of the matrix expression for the distribution of λ_1 as given by (3.1) are amenable to some cancellation by substitution. Consider the change of variable of integration given by $t \to a + u\sqrt{2a}$. This results in matrix elements of the form

$$\begin{aligned}
\Psi_{ij}(x) &= \sqrt{2a}\sqrt{\frac{i!j!}{(a+i)!(a+j)!}} \times \\
&\int_{-\sqrt{\frac{a}{2}}}^{y(x)} L_i^{(a)}(a+u\sqrt{2a}) L_j^{(a)}(a+u\sqrt{2a})(a+u\sqrt{2a})^a e^{-(a+u\sqrt{2a})} du \\
&= \sqrt{2a} a^a e^{-a} \sqrt{\frac{i!j!}{(a+i)!(a+j)!}} \times \\
&\int_{-\sqrt{\frac{a}{2}}}^{y(x)} L_i^{(a)}(a+u\sqrt{2a}) L_j^{(a)}(a+u\sqrt{2a})(1+u\sqrt{2/a})^a e^{-u\sqrt{2a}} du
\end{aligned} \quad . \tag{3.2}$$

Next, the behavior of the leading constants is examined, and it is noted that through some manipulation it is possible to cancel the extremely large terms in order to compute values exactly. Consider that these constants can be consolidated into

the form

$$\begin{aligned}
&\sqrt{2a}a^a e^{-a}\sqrt{\frac{i!j!}{(a+i)!(a+j)!}} \\
&= \frac{\sqrt{2a}a^a e^{-a}}{a!a^{i/2}a^{j/2}\sqrt{\Pi_{k=1}^{i}(1+k/a)\Pi_{k=1}^{j}(1+k/a)}} \\
&= \frac{1}{\sqrt{\pi}}a^{-i/2}a^{-j/2}\frac{e^{-\epsilon(a)}}{\sqrt{\Pi_{k=1}^{i}(1+k/a)\Pi_{k=1}^{j}(1+k/a)}}
\end{aligned}$$

where the function ϵ is defined by

$$\epsilon(a) = \log a! - a\log a + a - \frac{1}{2}\log 2\pi a.$$

Note that this equation can easily be computed to any arbitrary accuracy with the quickly converging series

$$\epsilon(a) = \frac{1}{12a} - \frac{1}{360a^3} + \frac{1}{1260a^5} - \frac{1}{1680a^7} + \dots.$$

Next, denote

$$c_{ij}(a) = \frac{e^{-\epsilon(a)}}{\sqrt{\Pi_{k=1}^{i}(1+k/a)\Pi_{k=1}^{j}(1+k/a)}}$$

and observe that $\lim_{a\to\infty} c_{ij}(a) = 1$. With this notation, the leading constant can be written as

$$\frac{1}{\sqrt{\pi}}a^{-i/2}a^{-j/2}c_{ij}(a)e^{-\epsilon(a)}.$$

As the leading constants have been consolidated into a tractable form, consider the terms originally arising from the gamma functions left in the integrand as a result of the change of variables and factorization of all constants. Define the function

$$\phi_a(t) = a\log(1 + t\sqrt{2/a}) - t\sqrt{2a}.$$

Note that for $|t| < \sqrt{a/2}$, this can be expanded in a Taylor series as

$$\phi_a(t) = -t^2 - \sum_{j=3}^{\infty}\frac{(-1)^j}{j}(t\sqrt{2/a})^j.$$

Combining these pieces, an elements of the matrix Ψ can be written

$$\begin{aligned}\Psi_{ij}(x) &= \frac{1}{\sqrt{\pi}} a^{-i/2} a^{-j/2} c_{ij}(a) e^{-\epsilon(a)} \\ &\times \int_{-\sqrt{\frac{a}{2}}}^{y(x)} L_i^{(a)}(a + u\sqrt{2a}) L_j^{(a)}(a + u\sqrt{2a}) e^{\phi_a(u)} du\end{aligned} \tag{3.3}$$

such that $y(x) = \frac{x-a}{\sqrt{2a}}$.

3.1.3 Asymptotics of Generalized Laguerre Polynomials

Prior to continuing the derivation, consider the relation between the generalized Laguerre and Hermite polynomials shown in [27]:

$$\lim_{a\to\infty} a^{-n/2} L_n^{(a)}(a + t\sqrt{a}) = \frac{(-1)^n}{n!} 2^{-n/2} H_n(t/\sqrt{2}).$$

Define polynomials

$$D_n^{(a)}(t) = (-1)^n n! (2/a)^{n/2} L_n^{(a)}(a + t\sqrt{2a}). \tag{3.4}$$

As a consequence of the Laguerre recurrence relation

$$L_{n+1}^{(a)}(x) = \frac{(2n + 1 + a - x)}{n+1} L_n^{(a)}(x) - \frac{(n+a)}{n+1} L_{n-1}^{(a)}(x),$$

the polynomials $D_n^{(a)}$ satisfy the recurrence relation

$$\begin{aligned} D_{n+1}^{(a)}(x) &= \left(2x - (2n+1)\sqrt{2/a}\right) D_n^{(a)}(x) - \left(2n + n^2(2/a)\right) D_{n-1}^{(a)}(x) \\ D_0^{(a)}(x) &= 1 \qquad\qquad D_1^{(a)}(x) = 2x - \sqrt{2/a}. \end{aligned} \tag{3.5}$$

Taking the limit $a \to \infty$, this recurrence relation is the same as that satisfied by the Hermite polynomials, with the same initial conditions. Therefore

$$\lim_{a\to\infty} D_n^{(a)} = H_n. \tag{3.6}$$

These polynomials are orthogonal on the interval $[-\sqrt{a/2}, \infty)$ with respect to the measure $e^{\phi_a(t)} dt$; i.e.,

$$\int_{-\sqrt{a/2}}^{\infty} D_n^{(a)}(t) D_m^{(a)}(t) e^{\phi_a(t)} dt = \frac{\sqrt{\pi} 2^n n!}{c_{nn}(a)} \delta_{nm}.$$

3.1.4 Closed Form D Polynomial Distribution

Substituting the D polynomials defined in Section 3.1.3 into the integral form of the matrix elements shown in (3.3) gives the matrix elements in terms of partial inner products of the D polynomials:

$$\Psi_{ij}(x) = \frac{c_{ij}(a)}{\sqrt{\pi 2^{i+j} i! j!}} \int_{-\sqrt{a/2}}^{y(x)} D_{i-1}^{(a)}(t) D_{j-1}^{(a)}(t) e^{\phi_a(t)} dt.$$

where as before, $y(x) = \frac{x-a}{\sqrt{2a}}$. The distribution can now be computed by taking the determinant of this matrix:

$$F_{\lambda_1}^{\mathcal{H}_0}(x) = \left| \frac{c_{ij}(a)}{\sqrt{\pi 2^{i+j} i! j!}} \int_{-\sqrt{a/2}}^{y(x)} D_i(t) D_j(t) e^{\phi_a(t)} dt \right|_{i,j=0,\ldots,M-1}. \tag{3.7}$$

This equation is tractable for computing probabilities in double precision arithmetic. Note that the D polynomial coefficients are precomputed using the recursion relation given by (3.5). The extremely large leading terms on each element of this matrix have been eliminated. Remaining factorial terms $i!j!$ are of order $M!$, which in the motivational cases of multistatic passive radar applications is a relatively small number, generally no larger than ten. Recall also that $c_{ij} \to 1$; as such the leading constant is very reasonable to compute using floating point arithmetic. Unlike the original measure $t^a e^{-t} dt$ associated with the gamma functions, the measure $e^{\phi_a(t)} dt$ does not cause double precision overflows for either modest or large values of a.

3.1.5 Asymptotic Hermite Polynomials

Note that computing the matrix elements, while numerically tractable using (3.7), may be computationally intensive due to the numerical integration required. In Section 3.1.3, it was noted when defining the D polynomials that as $a \to \infty$ in (3.6), $D_n^{(a)} \to H_n$. Therefore, the distribution of λ_1 can be written in terms of the Hermite

polynomials as

$$F_{\lambda_1}^{\mathcal{H}_0}(x) = \left| \frac{1}{\sqrt{\pi 2^{i+j} i! j!}} \int_{-\infty}^{y(x)} H_{i-1}(t) H_{j-1}(t) e^{-t^2} dt \right| \tag{3.8}$$

where as before, $y(x) = \frac{x-a}{\sqrt{2a}}$. With some additional recurrence relations, the elements of this matrix can be computed without computing any integrals. First, consider that $d(H_j(t)e^{-t^2}) = -H_{j+1}(t)e^{-t^2}$. For the zeroth row of the matrix, the inner product takes the form

$$\int_{-\infty}^{x} H_i(t) H_j(t) e^{-t^2} dt = \begin{cases} \sqrt{\pi}(1 + \mathrm{erf}(x))/2 & \text{if } j = 0 \\ -H_{j-1}(x) e^{-x^2} & \text{otherwise.} \end{cases}$$

Subsequent elements of the matrix can be recursively calculated using the relation

$$\int_{-\infty}^{x} H_i(t) H_j(t) e^{-t^2} dt = -H_i(x) H_{j-1}(x) e^{-x^2} + 2i \int_{-\infty}^{x} H_{i-1}(t) H_{j-1} e^{-t^2} dt.$$

The formulation of the distribution shown in (3.8) eliminates the large gamma functions with number of degrees of freedom (samples), thus eliminating the main cause of the severe floating point overflow. In addition, the recursion relations allows the elements of the matrix required to compute F_{λ_1} to be computed without employing a numerical integration algorithm. In cases where N is deemed sufficiently large that the error inherent in taking this limit is minimal, this recursive relation that relies on polynomial evaluation and highly optimized built in functions (such as the error function) as opposed to using numerical integration for evaluation can result in significant computational savings.

3.2 Derivation for the $\mathcal{H}_1$ Distribution

This section derives an expression for the distribution of λ_1 under the alternative hypothesis $\mathcal{H}_1$ that is numerically tractable for computation of probabilities in the

regimes of interest for the passive radar signal model presented in Section 2.1, i.e. in which the number of samples N is large and the number of distributed receivers M is relatively small. The methodology uses the fact that the matrix elements in the classical expressions for the CDF are incomplete gamma functions (with an extra hypergeometric term in the first column), and the relation to the orthogonality of the generalized Laguerre polynomials.

3.2.1 Laguerre Polynomial Conjugation

Recall the expression given for the non-central CDF of λ_1 in terms of gamma and hypergeometric functions, as shown in (2.17).

$$F_{\lambda_1}^{\mathcal{H}_1}(x) = \frac{1}{C}\left|\begin{cases} \int_0^x {}_0F_1(N-M+1,\mu_j t)t^{N-i+1}e^{-t}dt, \\ \qquad j=0,\ldots,K-1, i=0,\ldots,M-1 \\ \int_0^x t^{N-M+i+j+1}e^{-t}dt, \\ \qquad j=K,\ldots,M, i=0,\ldots,M-1 \end{cases}\right|.$$

Let $\Xi(x)$ be the $M \times M$ matrix given in the determinant form of $F_{\lambda_1}^{\mathcal{H}_1}$ shown above, and let A be the lower triangular matrix of normalized (in the Laguerre inner product sense) coefficients for the generalized Laguerre polynomials $L_i^{(a)}$ where the parameter $a = N - M$. Under the $\mathcal{H}_1$ hypothesis, $M-1$ columns of $\Xi(x)$ contain incomplete gamma functions. Thus, similar to the central case, conjugating $\Xi(x)$ by A followed by well chosen variable changes will allow cancellation of the extremely large intermediate terms generated by the gamma and hypergeometric functions in the matrix entries.

Consider the conjugation of $\Xi(x)$ by A, denoted $\Psi(x) = A^\dagger \Xi(x) A$. Note that the

CDF of λ_1 can be written as

$$\begin{aligned} F_{\lambda_1}^{\mathcal{H}_1}(x) &= \frac{|\Xi(x)|}{|\Xi(\infty)|} \\ &= \frac{\left|A^\dagger \Xi(x) A\right|}{|A^\dagger \Xi(\infty) A|} \\ &= \frac{|\Psi(x)|}{|\Psi(\infty)|}. \end{aligned}$$

An arbitrary element of the matrix $\Psi(x)$ is given by

$$\Psi_{ij}(x) = \sum_{l=i}^{M} \bar{A}_{il} \sum_{k=j}^{M} \Xi_{lk}(x) A_{kj}.$$

Note that due to the lower triangular structure of A, any terms in the summation where $l < i$ and $k < j$ are zero. This expansion may be divided into two cases: the first column containing hypergeometric function terms, and the other $M-1$ columns containing only incomplete gamma functions. First, consider the case that $j = 1$. Substituting the elements of $\Xi(x)$ and the corresponding generalized Laguerre coefficients constituting the elements of A into the above summation results in

$$\begin{aligned} \Psi_{ij}(x) = \sqrt{\frac{i!j!}{(a+i)!(a+j)!}} \sum_{l=i}^{M} \Bigg(& L_{M-i,M-l}^{(a)} L_{M-1,M-1}^{(a)} \\ & \int_0^x e^{-t} {}_0F_1(a+1, \mu_1 t) t^{N-l} dt \\ & + \sum_{k=2}^{M} L_{M-i,M-l}^{(a)} L_{M-1,M-k}^{(a)} \int_0^x e^{-t} t^{N+M-l-k} \Bigg) dt. \end{aligned}$$

In this expression $L_{i,j}^{(a)}$ denotes the coefficient corresponding to the t^j term of the generalized Laguerre polynomial $L_i^{(a)}$. Next, rearrange the sums and integrals, pulling

the factor of $e^{-t}t^{N-M} = e^{-t}t^a$ out from each term in the summations. This yields

$$\Psi_{ij}(x) = \sqrt{\frac{i!j!}{(a+i)!(a+j)!}} \int_0^x e^{-t}t^a \times$$
$$\sum_{l=i}^{M} \Big(L^{(a)}_{M-i,M-l} L^{(a)}_{M-1,M-1} {}_0F_1(N-M+1, \mu_1 t) t^{M-l}$$
$$+ \sum_{k=2}^{M} L^{(a)}_{M-i,M-l} L^{(a)}_{M-1,M-k} t^{2M-l-k} \Big)\, dt.$$

In this form, it is clear that to make computation of $\Psi_{ij}(x)$ numerically tractable, the leading integrand term arising from the incomplete gamma functions and the leading constants on the order of $a!$ must be eliminated. This is accomplished through a change of variables, substituting $t \to a + u\sqrt{2a}$. Making this substitution, the elements become

$$\Psi_{ij}(x) = \sqrt{\frac{i!j!}{(a+i)!(a+j)!}} \times$$
$$\int_{-\sqrt{a/2}}^{y(x)} e^{-(a+u\sqrt{2a})} (a+u\sqrt{2a})^a$$
$$\times \sum_{l=i}^{M} L^{(a)}_{M-i,M-l} L^{(a)}_{M-1,M-1}$$
$$\times {}_0F_1(a+1, \mu_1(a+u\sqrt{2a}))(a+u\sqrt{2a})^{M-l}$$
$$+ \sum_{k=2}^{M} L^{(a)}_{M-i,M-l} L^{(a)}_{M-1,M-k} (a+u\sqrt{2a})^{2M-l-k} \sqrt{2a}\, du$$

where $y(x) = \frac{x-a}{\sqrt{2a}}$. Factoring additional constant terms introduced by the substitution, the expression becomes

$$\Psi_{ij}(x) = \sqrt{2a}a^a e^{-a}\sqrt{\frac{i!j!}{(a+i)!(a+j)!}}\times \tag{3.9}$$
$$\int_{-\sqrt{a/2}}^{y(x)} e^{-u\sqrt{2a}}(1+u\sqrt{2/a})^a$$
$$\times \sum_{l=i}^{M} L^{(a)}_{M-i,M-l} L^{(a)}_{M-1,M-1}$$
$$\times {}_0F_1(a+1, \mu_1(a+u\sqrt{2a}))(a+u\sqrt{2a})^{M-l}$$
$$+ \sum_{k=2}^{M} L^{(a)}_{M-i,M-l} L^{(a)}_{M-1,M-k}(a+u\sqrt{2a})^{2M-l-k}\, du.$$

(3.10)

3.2.2 Computing the Matrix Elements

Note that the expression $F_{\lambda_1}(x) = |\Psi|$ is exact, but computing the matrix elements Ψ_{ij} still presents difficulties. In particular, the factor multiplying the integral in (3.9) contains factorials of the number of samples. This section develops a numerically tractable form that allows for computation to an arbitrary accuracy by using further terms of the convergent series. Consider the leading constant in (3.9). Applying Stirling's approximation yields

$$\begin{aligned}
&\sqrt{2a}a^a e^{-a}\sqrt{\frac{i!j!}{(a+i)!(a+j)!}} \\
&= \frac{\sqrt{2a}a^a e^{-a}}{a!a^{i/2}a^{j/2}\sqrt{\Pi_{k=1}^{i}(1+k/a)\Pi_{k=1}^{j}(1+k/a)}} \\
&= \frac{1}{\sqrt{\pi}}a^{-i/2}a^{-j/2}\frac{e^{-\epsilon(a)}}{\sqrt{\Pi_{k=1}^{i}(1+k/a)\Pi_{k=1}^{j}(1+k/a)}}
\end{aligned}$$

where the function ϵ is defined by

$$\begin{aligned}
\epsilon(a) &= \log a! - a\log a + a - \frac{1}{2}\log 2\pi a \\
&= \frac{1}{12a} - \frac{1}{360a^3} + \frac{1}{1260a^5} - \frac{1}{1680a^7} + \dots.
\end{aligned}$$

Denote

$$c_{ij}(a) = \frac{e^{-\epsilon(a)}}{\sqrt{\Pi_{k=1}^{i}(1+k/a)\Pi_{k=1}^{j}(1+k/a)}}$$

and observe that $\lim_{a\to\infty} c_{ij}(a) = 1$. Next, define

$$\phi_a(t) = a\log(1+t\sqrt{2/a}) - t\sqrt{2a}.$$

For $|t| < \sqrt{a/2}$, this can be expanded in a Taylor series as

$$\phi_a(t) = -t^2 - \sum_{j=3}^{\infty} \frac{(-1)^j}{j}(t\sqrt{2/a})^j.$$

Using these functions, the CDF may be written in the form

$$\Psi_{ij}(x) = \frac{c_{ij}(a)a^{-i/2}a^{-j/2}\sqrt{i!j!}}{\sqrt{\pi}} \int_{-\sqrt{a/2}}^{y(x)} e^{\phi_a(u)} \tag{3.11}$$

$$\sum_{l=i}^{M} L^{(a)}_{M-i,M-l} L^{(a)}_{M-1,M-1}$$

$$\times\, {}_0F_1(a+1, \mu_1(a+u\sqrt{2a}))(a+u\sqrt{2a})^{M-l}$$

$$+ \sum_{k=2}^{M} L^{(a)}_{M-i,M-l} L^{(a)}_{M-1,M-k}(a+u\sqrt{2a})^{2M-l-k} du. \tag{3.12}$$

3.2.3 The Distribution

Recall the family of D polynomials defined in Section 3.1.3, defined by the following relationship with the Laguerre polynomials

$$D_n^{(a)}(t) = (-1)^n n!(2/a)^{n/2} L_n^{(a)}(a+t\sqrt{2a}).$$

Substituting the coefficients for the D polynomials in place of the generalized Laguerre polynomial coefficients into the form of the matrix elements Ψ_{ij} given in

(3.11) results in

$$\begin{aligned}\Psi_{ij}(x) = & \frac{c_{ij}(a)}{\sqrt{\pi 2^{i+j} i! j!}} \int_{-\sqrt{a/2}}^{y(x)} e^{\phi_a(u)} \\ & \sum_{l=i}^{M} D^{(a)}_{M-i,M-l} D^{(a)}_{M-1,M-1} u^{M-l} \\ & {}_0F_1(a+1, \mu_1(a+u\sqrt{2a})) \\ & + \sum_{k=2}^{M} D^{(a)}_{M-i,M-l} D^{(a)}_{M-1,M-k} u^{2M-l-k} du.\end{aligned} \tag{3.13}$$

This completes the calculation. Next, consider the elements $\Psi_{ij}(x)$ for the case $j = 2, \ldots, M$. It is clear the derivation will follow as shown in this section, without the hypergeometric function in the leading part of the summation. This allows these elements to be written more concisely as partial inner products of the D polynomials.

$$\Psi_{ij}(x) = \frac{c_{ij}(a)}{\sqrt{\pi 2^{i+j} i! j!}} \int_{-\sqrt{a/2}}^{y(x)} D^{(a)}_{i-1}(t) D^{(a)}_{j-1}(t) e^{\phi_a(t)} dt \tag{3.14}$$

Therefore, the cumulative distribution function for λ_1 can be written as the determinant of Ψ; i.e.,

$$F^{\mathcal{H}_1}_{\lambda_1}(x) = |\Psi_{ij}(x)| \tag{3.15}$$

such that the matrix elements $\Psi_{ij}(x)$ are given by (3.13) and (3.14). [28].

3.2.4 Perturbation Formula for the Distribution

It is of interest to determine an exact relationship between the distribution of λ_1 under the $\mathcal{H}_0$ and $\mathcal{H}_1$ hypotheses. This section presents a formula for the distribution under $\mathcal{H}_1$ equivalent to that given in (3.15), written as a rank one perturbation of the distribution under $\mathcal{H}_0$ as given by (3.7). Techniques similar to those employed in both cases to make the distributions amenable to floating point computation are used on the perturbation term to allow closed form computation of the $\mathcal{H}_1$ distribution

using this method. Further, asymptotic results are discussed, in order to present an approximation of the $\mathcal{H}_1$ distribution that is analogous to the Hermite polynomial form of the $\mathcal{H}_0$ distribution as given by (3.8).

Let $\Xi(x)$ be the matrix given by (2.17). Recall the the distribution of λ_1 under $\mathcal{H}_1$ can be written

$$F_{\lambda_1}^{\mathcal{H}_1}(x) = \frac{|\Xi(x)|}{|\Xi(\infty)|}.$$

Let A be the lower triangular matrix of generalized Laguerre polynomial coefficients of order $a = N-M$, and let $\Psi(x)$ be the matrix of incomplete Laguerre inner products as given by (3.1). Then Ξ can be written as a rank one perturbation of Ψ.

$$A\Xi(x)A^T = \Psi(x) + v(x)\ell^T \tag{3.16}$$

such that ℓ is the first column of A, i.e., the coefficients of the generalized Laguerre polynomial of degree $M-1$. The elements of the vector $v(x)$ are given by

$$v_j(x) = \frac{j!}{(a+j)!}\int_0^x \left({}_0F_1(a+1,\mu_1 t) - 1\right) L_j^{(a)} t^a e^{-t} dt. \tag{3.17}$$

Recall the matrix determinant lemma, which in the special case of a rank-1 perturbation, states

$$\left|A + uv^T\right| = \left(1 + v^T A^{-1} u\right)|A|.$$

Applying this lemma to (3.16), it is then possible to rewrite $F_{\lambda_1}^{\mathcal{H}_1}$ as

$$F_{\lambda_1}^{\mathcal{H}_1}(x) = \frac{1 + \ell^T \Psi^{-1}(x) v(x)}{1 + \ell^T v(\infty)} |\Psi(x)|.$$

Recall that $F_{\lambda_1}^{\mathcal{H}_0}(x) = |\Psi(x)|$. Therefore, it is possible to rewrite $F_{\lambda_1}^{\mathcal{H}_1}$ as a perturbation of $F_{\lambda_1}^{\mathcal{H}_0}$.

$$F_{\lambda_1}^{\mathcal{H}_1}(x) = \frac{1 + \ell^T \Psi^{-1}(x) v(x)}{1 + \ell^T v(\infty)} F_{\lambda_1}^{\mathcal{H}_0}(x) \tag{3.18}$$

The perturbation formula for the CDF of λ_1 under $\mathcal{H}_1$ given by (3.18) is susceptible to the double precision arithmetic overflow problems previously discussed and addressed in [26, 28], but may likewise be addressed with similar methods. In particular, it is necessary to address the numerical overflow problem in the $\Psi^{-1}(x)$, $v(x)$, and $F_{\lambda_1}^{\mathcal{H}_1}(x)$ terms of (3.16). Clearly, $F_{\lambda_1}^{\mathcal{H}_1}(x)$ and by extension Ψ^{-1} may be computed using the D or Hermite polynomial CDF equations presented in [26]. This section will discuss a similar argument for computing the elements of v in terms of partial inner products of D polynomials, along with some discussion of an asymptotic expression in terms of Hermite polynomials and how the hypergeometric function terms behave in these regimes.

Consider the vector $v(x)$ as defined in (3.17). By following a procedure similar to the arguments originally seen in [26], by making the substitution $t \to a + t\sqrt{2a}$ it is possible to reformulate $v(x)$ in a way that avoids the numerical overflow problems seen in the integrals encountered in this problem. In particular, elements of $v(x)$ may be written

$$v_j(x) = \frac{c_j(a)}{\sqrt{\pi 2^j j!}} \int_{-\sqrt{a/2}}^{y(x)} e^{\phi_a(t)} \left({}_0F_1(a+1, \mu_1 t) - 1 \right) D_j^{(a)}(t) dt \qquad j = 0, \ldots, M-1 \tag{3.19}$$

such that $y(x) = \frac{x-a}{\sqrt{2a}}$, the polynomials $D_n^{(a)}$ and function $\phi_a(t)$ are as defined in [26, 28], and

$$c_j(a) = \frac{e^{-\epsilon(a)}}{\sqrt{\prod_{k=1}^{j}(1 + k/a)}}$$

with $\epsilon(a)$ again as defined in [26, 28].

This work is motivated by passive radar problems in which the degrees of freedom

N represents the number of samples, i.e., the time-bandwidth product of the captured data, and can be quite large, while the size of the Wishart distribution M represents the number is receivers and is generally considered to be small. Thus it is of interest to consider asymptotic expressions for the distribution of λ_1 in the case of $N \to \infty$. Arguments were presented in [26] for an asymptotic form of the distribution of λ_1 in terms of the Hermite polynomials, as $D_j^{(a)}(t) \to H_n(t)$. Through the use of recurrence relations, this allows the distribution under $\mathcal{H}_0$ to be approximated without the use of numerical integration algorithms, resulting in a substantial savings in computation time. It is of interest to attempt a similar methodology in the $\mathcal{H}_1$. Using the perturbation formula given in (3.16), the distribution $F_{\lambda_1}^{\mathcal{H}_0}$ and $\Psi^{-1}(x)$ can be computed using the Hermite polynomial forms defined in [26]. Taking some limits in N in the $v(x)$ term results in the expression

$$v_j(x) = \frac{1}{\sqrt{\pi 2^j j!}} \int_{-\infty}^{y(x)} e^{-x^2} \left({}_0F_1(a+1, \mu_1 t) - 1\right) H_{j-1}(t) dt \qquad j = 1, \ldots, M. \quad (3.20)$$

Note that the limit has deliberately not been taken in the hypergeometric term ${}_0F_1$, as for constant μ_1, ${}_0F_1(a+1, \mu_1 t) \to 1$ and therefore $F_{\lambda_1}^{\mathcal{H}_1}(x) \to F_{\lambda_1}^{\mathcal{H}_0}(x)$, but in regimes of interest, clearly this is not a good approximation, i.e., the large value of $a = N - M$ does not outweigh the influence of μ_1, and the ${}_0F_1$ term does not converge to 1.

3.3 Derivation of the Correlated Central Distribution

Using the methods demonstrated in the previous two sections, it is possible to construct a computationally tractable form of the distribution of λ_1 in the case of a correlated central Wishart matrix, which is the distribution of $X^\dagger X$ when X is zero mean complex Gaussian with an arbitrary covariance matrix Σ. λ_1 is not generally the GLRT for various detection problems of interest where the data follows a correlated Gaussian distribution under one or both of the hypotheses, e.g., in which the

signal under $\mathcal{H}_1$ is modeled as being in the covariance rather than the mean. Similarly, in cases where the signal is in the mean but the noise has some non-identity covariance, the GLRT is a function of the trace and thus depends on all M eigenvalues [20]. Nevertheless, there is interest in the distribution in the MIMO communications literature, where it may arise in models of spatial correlation across multiple channels at either the transmit or receive antennas [21], and in some practical engineering cases performance may be close enough to the more optimal choice that the largest eigenvalue may be used as a statistic when some more complicated function of the eigenvalues may be costly to compute or too difficult to characterize.

3.3.1 Known CDF of λ_1

Theorem 2 implies that the CDF of λ_1 can be written as the determinant of some matrix if it is possible to express the PDF in terms of some matrices $\Psi(x)$, $\Phi(x)$, and functions $\xi(x)$. These are known for the uncorrelated central, correlated central, and uncorrelated non-central cases, and are given in [3]. In particular, for the central correlated case, the matrix elements are

$$\phi_i(x_j) = x_j^{M-i}$$

and

$$\psi_i(x_j) = e^{-x_j/\sigma_i}.$$

The function ξ is

$$\xi(x_k) = x_k^{N-M}.$$

Therefore, using the lemma, the CDF of λ_1 can be written as

$$F_{\lambda_1}^{\Sigma}(x) = \frac{1}{C}\left|\int_0^x t^{N-M+i}e^{-t/\sigma_j}dt\right|_{i,j=0,\ldots,M-1} \tag{3.21}$$

such that C is a normalizing constant equal to the limit of the determinant term as $x \to \infty$. Performing the substitution of $u = t/\sigma_j$, it is thus possible to rewrite F as

$$\begin{aligned} F_{\lambda_1}^{\Sigma}(x) &= \frac{1}{C}\left|\int_0^x t^{N-M+i}e^{-t/\sigma_j}dt\right|_{i,j=0,\ldots,M-1} \\ &= \frac{1}{C}\left|\int_0^{x/\sigma_i} (u\sigma_j)^{N-M+i}e^{-u}\sigma_j du\right|_{i,j=0,\ldots,M-1} \\ &= \frac{1}{C}\left|\sigma_j^{N-M+i}\int_0^{x/\sigma_j} u^{N-M+i+1}e^{-u}du\right|_{i,j=0,\ldots,M-1} \\ &= \frac{1}{C}\left|\sigma_j^{N-M+i+1}\gamma(N-M+i, x/\sigma_j)\right|_{i,j=1,\ldots,M-1}. \end{aligned} \tag{3.22}$$

Note that this matrix is not Hermitian, and as such, will present a less concise formulation when arguments similar to those used in [26] are applied. However, it is important to note the structure of the elements is generally very similar, and as such, it is possible to proceed as in the two previously examined cases.

3.3.2 Laguerre Polynomial Expansion

Starting with the form of $F_{\lambda_1}^{\Sigma}(x)$ presented in (3.22), it is possible to again apply the Laguerre polynomial conjugation procedure to allow us to compute the distribution for large values of N. Conjugate (3.21) with a triangular matrix of generalized Laguerre polynomial coefficients A with coefficient $a = N - M$, with the goals of eliminating the t^a integrand terms that cause the intermediate computational quantities in this distribution to be on the order of $a!$. As seen in the prior derivations,

let $\Xi(x)$ be the matrix in (3.22), and let $\Psi = A^{\dagger}\Xi A$. The elements of Ψ are

$$\Psi_{ij} = \sqrt{\frac{i!j!}{(a+i)!(a+j)!}} \sum_{l=i}^{M} \sum_{k=j}^{M} L^{(a)}_{M-i,M-l} L^{(a)}_{M-j,M-k} \sigma_k^l \int_0^{x/\sigma_k} t^i t^a e^{-t} dt \tag{3.23}$$

where $L^{(a)}_{i,j}$ signifies the order j coefficient of the order i generalized Laguerre polynomial. As previously seen, the leading constant of order $a!$ and the integrand term of order $t^a e^{-t} dt$ represent an extremely large numerical cancellation occurring on every intermediate term that one must compute when attempting to use this expression to compute values of this CDF. Thus it is again proposed to make a change of variables from $t \to a + u\sqrt{2a}$, which simultaneously allows for the consolidation and cancellation of large leading constants and changes the integral into something which can be computed for large values of N using numerical quadrature. Making this substitution and consolidating the constants as previously seen results in elements of Ψ taking the form

$$\begin{aligned} \Psi_{ij} = \frac{c_{ij}(a) a^{-i/2} a^{-j/2} \sqrt{i!j!}}{\sqrt{\pi}} \sum_{l=i}^{M} \sum_{k=j}^{M} L^{(a)}_{M-i,M-l} L^{(a)}_{M-j,M-k} \sigma_k^l \\ \times \int_0^{x/\sigma_k} (a + u\sqrt{2a})^i e^{-\phi_a(u)} du \end{aligned} . \tag{3.24}$$

The functions $c_{ij}(a)$ and $\phi_a(t)$ are as defined in Sections 3.1 and 3.2.

3.3.3 The Distribution

Recall the D polynomials defined in terms of the generalized Laguerre polynomials in Section 3.1.3.

$$D_n^{(a)}(t) = (-1)^n n! (2/a)^{n/2} L_n^{(a)}(a + t\sqrt{2a}).$$

The derivation of a reasonably concise and computable form for elements of the matrix Ψ is completed by making the substitution of the Laguerre polynomial coefficients for the D polynomial coefficients that are orthogonal over the new domain of

integration introduced by the substitution. The final expression for the coefficients of the matrix Ψ is given by

$$\Psi_{ij}(x) = \frac{c_{ij}(a)}{\sqrt{\pi 2^{i+j} i! j!}} \sum_{l=i}^{M} \sum_{k=j}^{M} D^{(a)}_{M-i,M-l} D^{(a)}_{M-j,M-k} \sigma_k^l \int_{-\sqrt{\frac{a}{2}}}^{y_{\sigma_k}(x)} e^{\phi_a(u)} (a + u\sqrt{2a})^{M-l+1} du. \tag{3.25}$$

The functions $c_{ij}(a)$ and $\phi_a(u)$ are as defined in Sections 3.1 and 3.2. Note however that the upper bound of each integral term in the summation is $y_{\sigma_k}(x) = \frac{x/\sigma_k - a}{\sqrt{2a}}$, which depends on k and thus cannot be factored out of the sum. This expression contains a large number of numerical integration terms that are not easily combined as in the other two cases, and could be potentially much more computationally costly as a result. It may be possible to rework this expression in such a matter that minimizes redundant computation, which is worthy of future attention.

Chapter 4

NUMERICAL RESULTS

This chapter presents a variety of numerical results related to the theoretical derivations of distributions seen in Chapter 3. The distributions of λ_1 under the $\mathcal{H}_0$ and $\mathcal{H}_1$ hypotheses constructed via the Laguerre polynomial expansion methods are compared with the well known expressions from the literature and empirically calculated distributions derived from Monte Carlo simulations in Sections 4.1.1 and 4.2.2. The $\mathcal{H}_0$ distribution formulas are then used to numerically compute detection thresholds in Section 4.1.2, and compared against Monte Carlo methods and the Tracy-Widom approximation in Section 4.1.3. Limitations of the $\mathcal{H}_1$ distribution formulas due to the numerical instability of the ${}_0F_1$ hypergeomtric function are discussed in Section 4.2.1. The viability of these formulas is demonstrated by using them to compute receiver operating characteristic curves in section 4.2.3. Discussion of the limited viability inherent to both direct Monte Carlo simulation and existing methods to reduce the number of pseudorandom trials required is presented in Section 4.3. Finally, a simulation of the multistatic passive radar problem presented in Section 2.1 is shown in Section 4.4, along with some discussion of practical engineering concerns and model limitations.

4.1 $\mathcal{H}_0$ Numerics

This section discusses using the expressions derived in the $\mathcal{H}_0$ to compute probabilities of λ_1 in the signal absent case, which may be used to set thresholds. This work was performed prior to work on the $\mathcal{H}_1$ case, meaning at the time only a "half-closed form" ROC was possible, i.e. in which the probability of false alarm are computed in

closed form while probability of detection is computed using Monte Carlo simulation. These results are included and discussed for sake of completeness.

4.1.1 CDF Comparison

In this section, the expressions introduced in Section 3.1 for $F_{\lambda_1}^{\mathcal{H}_0}(x)$ are compared to the classical formula for the distribution given in Section 2.4 for small problem sizes and to empirical estimates of the distribution generated using Monte Carlo trials for larger problem sizes where floating point overflow may occur. These plots were generated using MATLAB scripts which are documented in Appendix A. First, consider a case in which N is sufficiently small that the gamma expression for the distribution can be compared with the D polynomial formula derived in Section 3.1.

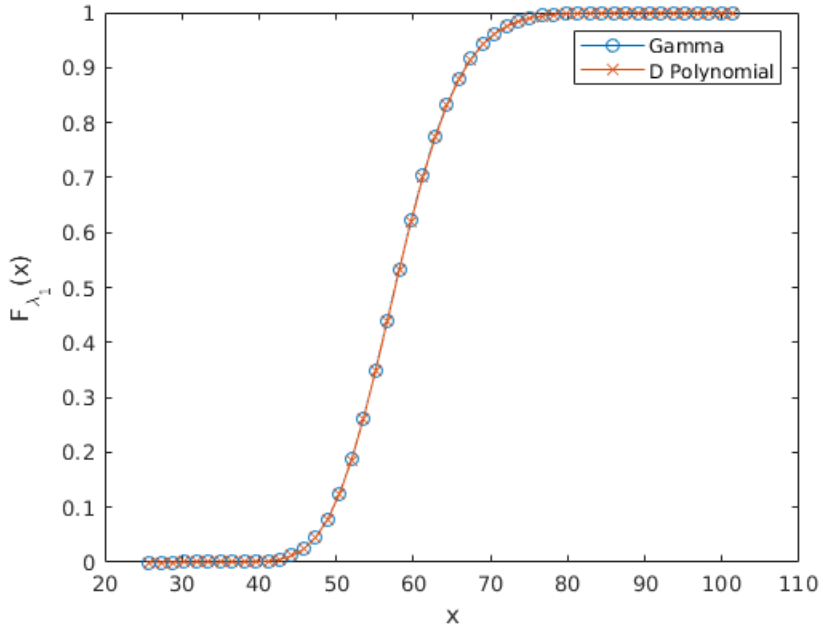

Figure 4.1: Central CDF Comparison from (2.15) and (3.7) for $M = 2$ and $N = 50$.

With $M = 2$ and $N = 50$, the two equations produce numerical results which have differences on the order of machine precision. Although this is not a particu-

larly useful example for the passive radar application motivating this work, Fig. 4.1 is a useful sanity check that the expression given by (3.7) is in fact exact. Next, consider a comparison with a problem with a larger N, which is likely more realistic for a multistatic passive radar application. In this case, (2.15) overflows double precision floating point representation and it is necessary to compare to an empirically estimated Monte Carlo CDF.

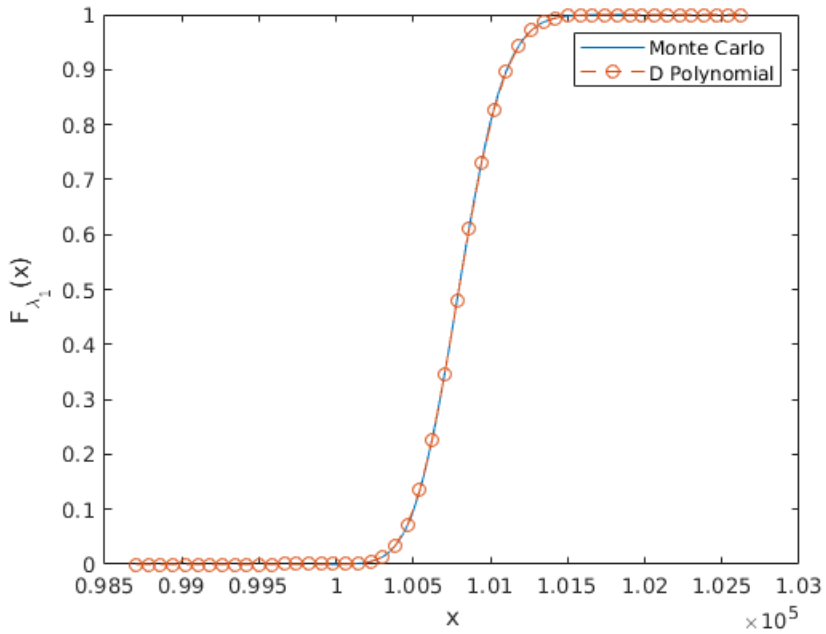

Figure 4.2: Central CDF Comparison Computed Using (3.7) and Monte Carlo Trials for $M = 2$ and $N = 10^5$ with 10^6 Trials.

The D polynomial CDF agrees with the Monte Carlo distribution to machine precision in the main body of the curve shown in Fig. 4.2. There is increased error further out into the tails of the distribution, as events become more rare and unlikely to occur in a modest sized Monte Carlo trial. Consider that it is of particular interest to compute values of the complementary CDF $1 - F_{\lambda_1}^{\mathcal{H}_0}(x)$ for characterization of the probability of false alarm P_F of a detector for a given operating threshold T in the tail of the distribution, corresponding to quite small values of P_F. The following plots

demonstrate the complementary CDF in ranges which are of interest for tolerable values of P_F, which is often within a few orders of magnitude of 10^{-9}. This is clearly not feasible using Monte Carlo approximations, due to the extremely large number of trials that would be required to obtain a reasonable estimate. Shown here are figures demonstrating the complementary CDF with $M = 2$ sensors and $N = 10^4$, as well as for $M = 5$ and $N = 10^6$, demonstrating the viability of the new methods to practical passive radar problems. Monte Carlo simulations with 10^6 trials at each point were performed.

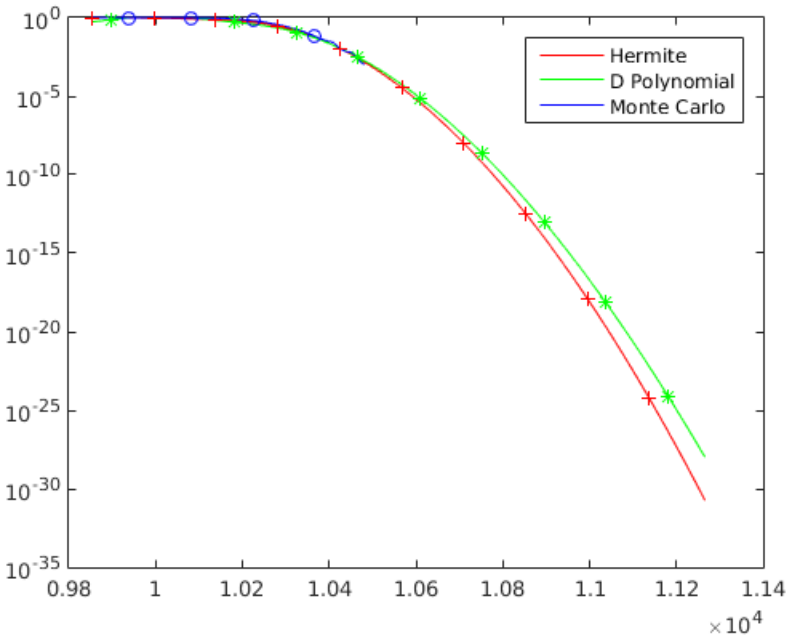

Figure 4.3: Complementary CDFs of Hermite polynomial (3.8) and D polynomial (3.7) formulas compared with Monte Carlo for $M = 2$ and $N = 10^4$.

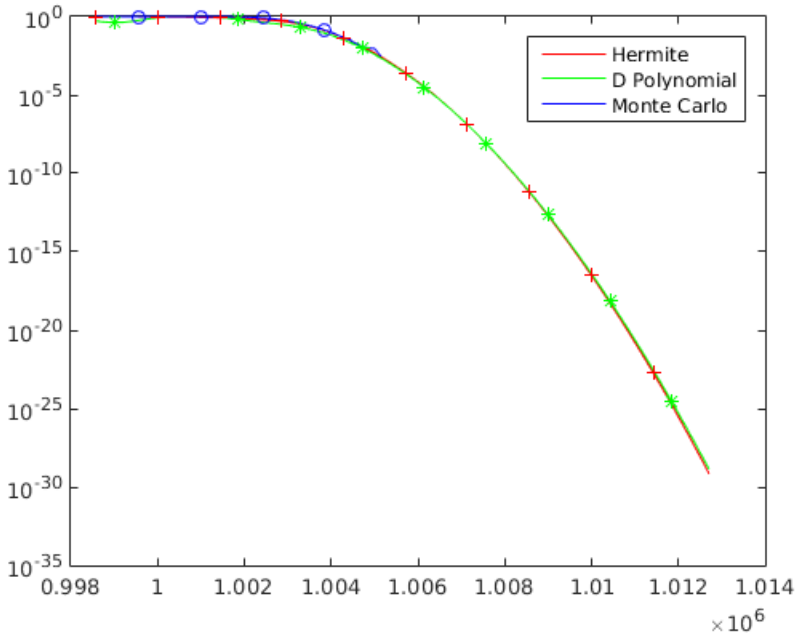

Figure 4.4: Complementary CDFs of Hermite polynomial (3.8) and D polynomial (3.7) formulas compared with Monte Carlo for $M = 5$ and $N = 10^6$.

The new methods agree with Monte Carlo simulation up to approximately one order of magnitude below the inverse of the number of trials performed, below which a Monte Carlo estimate is meaningless. Larger experiments would be too computationally time intensive. Note that in Fig. 4.3, for probability values down to approximately 10^{-9}, the Hermite and D polynomial methods are extremely close, with some divergence at lower orders of magnitude. This is expected, as the Hermite expression as given by (3.8) is asymptotic. In Fig. 4.4, with a larger value of N there is much closer agreement between the exact D polynomial and asymptotic Hermite expressions, down to probability values that are likely many orders of magnitude below a realistic operating P_F. In such a case, a fast algorithm taking advantage of the lack of numerical integration required for the Hermite expression may be advantageous.

4.1.2 Threshold Computation

A primary motivation in finding computationally tractable formulas for the distribution of λ_1 in the central case is to be able to explicitly compute threshold values for the binary hypothesis problem derived in Section 2.2. The exact and asymptotic distribution formulas shown in (3.7) and (3.8), respectively, can be used to compute detection threshold values T for a given probability of false alarm, defined as the probability the data (or equivalently, the sufficient statistic) exceeds the threshold T.

$$\begin{aligned} P_F &= \int_{T_X}^{\infty} p(X|\mathcal{H}_0)dX \\ &= \int_{T}^{\infty} p(\Lambda(X)|\mathcal{H}_0)d\Lambda(X) \\ &= 1 - F_{\lambda_1}^{\mathcal{H}_0}(T) \end{aligned}$$

T can be calculated to within a given tolerance of error on the probability of false alarm through iterative computation, or for given system operating thresholds performance may be characterized through exact calculation of P_F. First, consider an example in which thresholds for given false alarm rates are computed using the gamma function formula for the CDF $\mathcal{H}_0$ as seen in the literature or previously given by (2.15) compared with thresholds computed using the D polynomial formula given in (3.7). Due to the inherent numerical overflow problems with (2.15), the degrees of freedom N is quite limited in size in this problem.

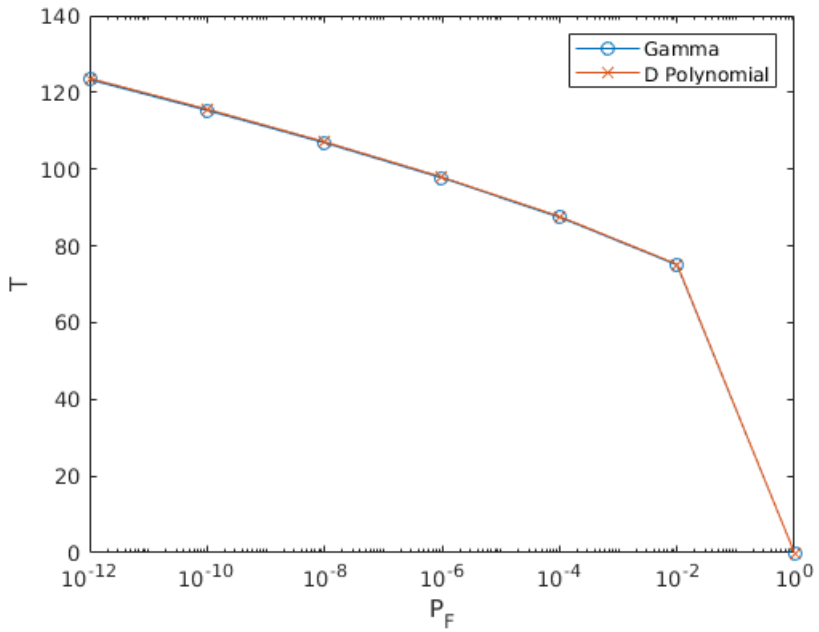

Figure 4.5: Threshold Values for a Given P_F Computed in Closed Form Using (2.15) and (3.7) for $M = 2$, $N = 50$.

Next, consider an example in which it is of interest to compute thresholds for a multistatic passive radar system in which it is desirable to record a large number of samples N to achieve an acceptable level of performance. This makes the use of (2.15) impossible; consequently it is necessary to compare the D polynomial expression for the distribution against computing thresholds with an empirical distribution generated through Monte Carlo trials. This presents its own difficulties, as realistic operational P_F values tend to be quite small, often on the order of 10^{-9} or smaller. To achieve an acceptable level of accuracy when estimating values with an empirical CDF generated using Monte Carlo methods, it is necessary to draw several orders of magnitude more samples than $1/P_F$. For these extremely small P_F values, this may be extremely computationally costly.

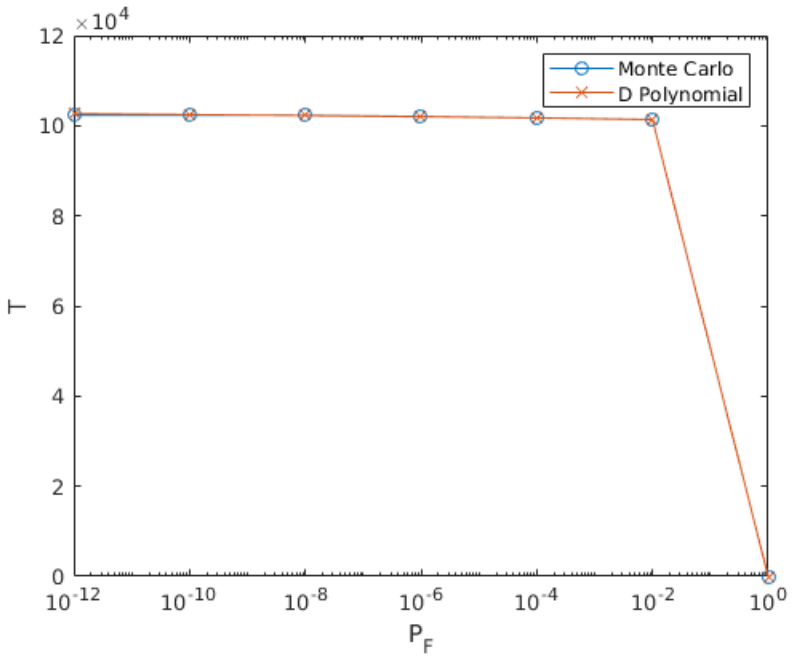

Figure 4.6: Threshold Values for a Given P_F Computed Using Monte Carlo Trials and (3.7) for $M = 4$, $N = 10^5$.

Per the computational cost of characterizing the tail of the distribution through Monte Carlo methods, the example plot shown in Fig. 4.6, the first three values for thresholds corresponding to P_F values of 10^{-12}, 10^{-10}, and 10^{-8} as found using an empirical estimate of the distribution using Monte Carlo methods are a lower bound, as only 10^8 trials were run in this experiment.

4.1.3 Tracy-Widom Comparison

The most well known asymptotic result in the literature for computing the distribution of λ_1 is the Tracy-Widom distribution [22]. These results derive a distribution for the asymptotic behavior of λ_1 as $N, M \to \infty$ at some constant fixed ratio $C = N/M$. It is acknowledged that these results provide an accurate approximation in regions of the distribution near to the mean, but are less accurate in the tails of the distribution, which is of primary interest in multi-channel detection for the purpose of

setting thresholds with low probability of false alarm. Consider Fig. 4.7 below which compares thresholds from a Monte Carlo simulation of 10^7 trials to those computed using (3.7) and using the Tracy-Widom distribution with algorithms available from [4].

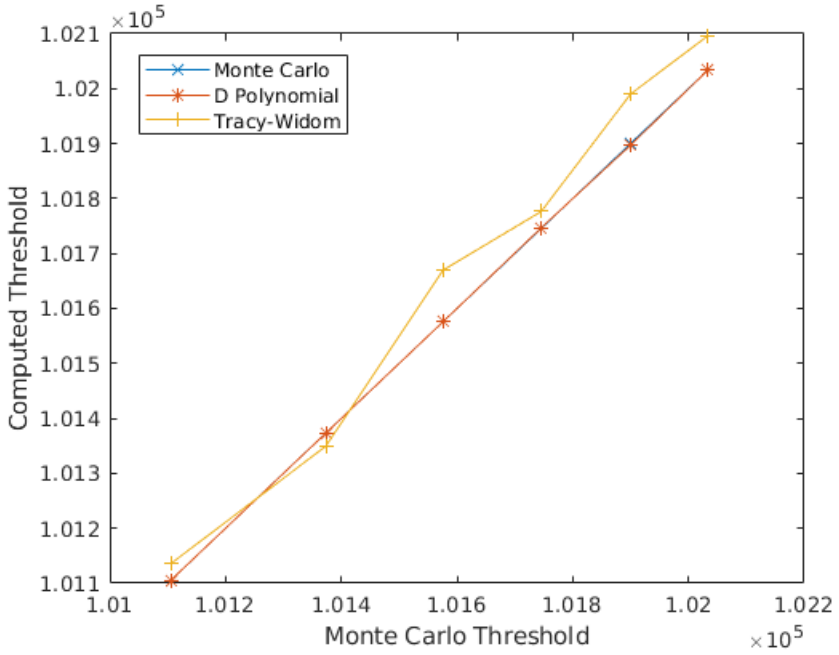

Figure 4.7: Thresholds Computed Using (3.7) and the Tracy-Widom Algorithms from [4] Against Thresholds Found from a Monte Carlo Simulation for $M = 4$ and $N = 10^5$, Corresponding to Probability of False Alarm Values 10^k Where $k = -6, \ldots, -1$

It is clear that the Tracy-Widom thresholds are much less accurate than those computed using (3.7), which is made even apparent in the following relative error plot.

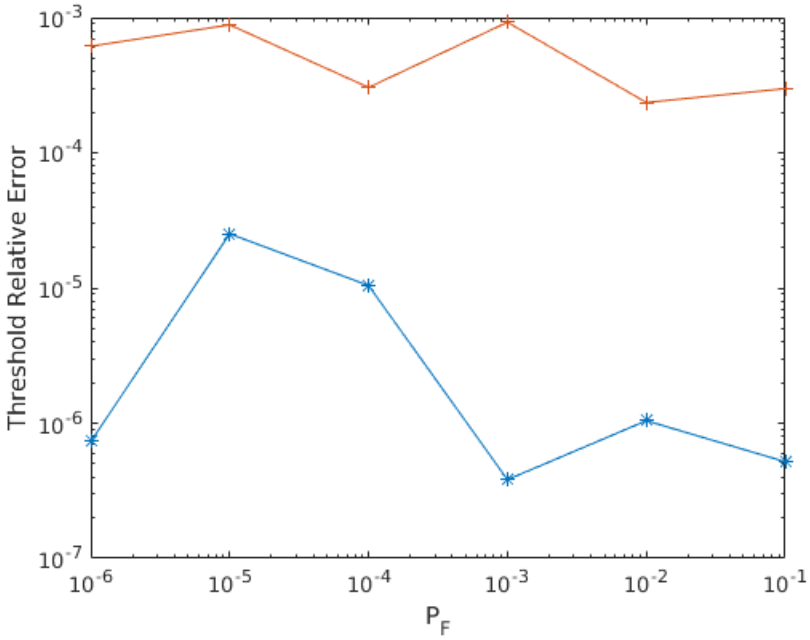

Figure 4.8: Relative Error of Thresholds Computed Using (3.7) and the Tracy-Widom Algorithms Against Thresholds Found from a Monte Carlo Simulation for $M = 4$ and $N = 10^5$, Corresponding to Probability of False Alarm Values 10^k Where $k = -6, \ldots, -1$

Similarly, by using the thresholds found from the Monte Carlo experiment as the arguments for the D polynomial and Tracy-Widom distribution algorithms, the expected values of P_F given by the corresponding models can be computed. These values are show in Fig. 4.9.

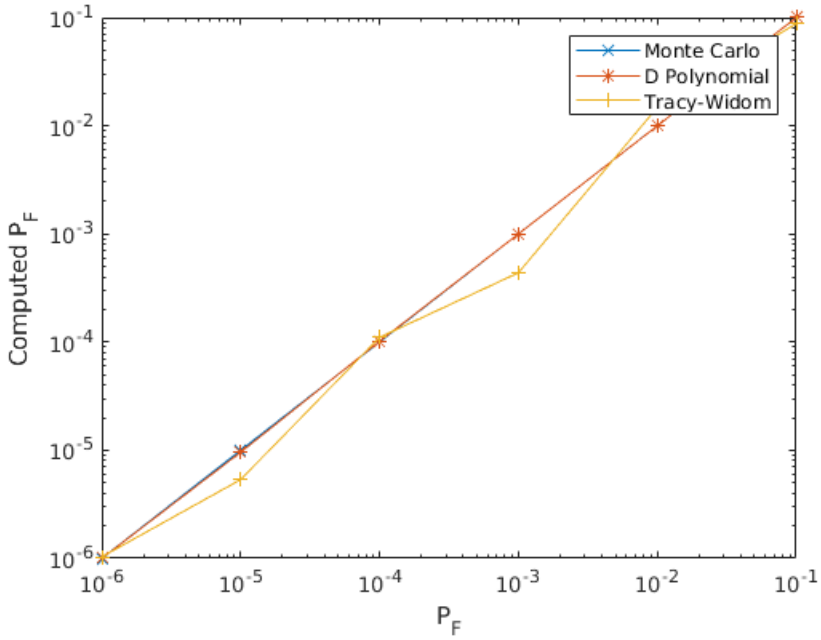

Figure 4.9: P_F Computed Using a Monte Carlo Experiment, (3.7), and the Tracy-Widom Algorithms for $M = 4$ and $N = 10^5$

As seen in the threshold case, the relative error between the true expected P_F and the values returned from the algorithm is several orders of magnitude higher in the Tracy-Widom case. Note that in the D polynomial case the error does increase for lower values of P_F; acquiring initial thresholds to use from a larger Monte Carlo experiment would likely decrease this significantly.

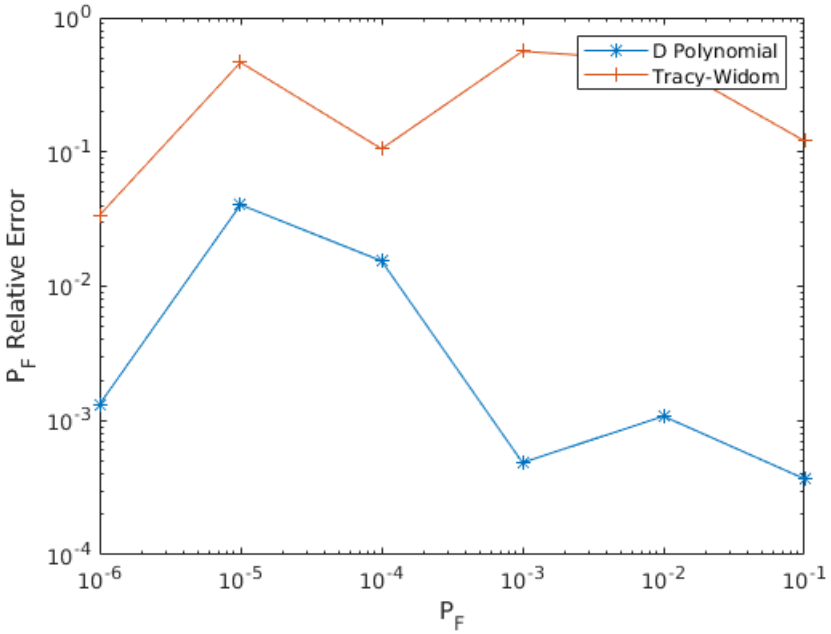

Figure 4.10: Relative Error of P_F Computed Using Monte Carlo Thresholds and the Tracy-Widom Algorithms and (3.7) Against Expected P_F for $M = 4$ and $N = 10^5$

.

4.1.4 Receiver Operating Characteristic

Receiver operating characteristic (ROC) curves can be computed by first computing the threshold as seen in Section 4.1.2, and subsequently calculating the probability of detection using the distribution under the $\mathcal{H}_1$ hypothesis.

$$\begin{aligned} P_D &= \int_{T_X}^{\infty} p(X|\mathcal{H}_1)dX \\ &= \int_{T}^{\infty} p(\Lambda(X)|\mathcal{H}_1)d\Lambda(X) \\ &= 1 - F_{\lambda_1}(T) \end{aligned}$$

It is typically desirable to characterize the performance of a detection system by viewing the probability of detection P_D as a function of the probability of false alarm P_F.

To compute an ROC curve in closed form, it is necessary to compute the distribution of the test statistic under the $\mathcal{H}_1$, in this case λ_1 in the non-central case. This problem has seen some attention in the literature [1, 29, 30, 31], including a closed form solution in terms of hypergeometric functions as seen in (2.17) [3]. However, known methods in the literature are not computationally tractable, encountering the same overflow problems as in the central case.

Prior to the introduction of the methods shown in Section 3.2, the only possible solution to generating an ROC curve would be to compute P_F in closed form using (3.7) and to estimate P_D through an empirical CDF generated using Monte Carlo simulations, the detector is lower bounded by the line $P_F = P_D$, and in a realistic use case would not operate in a regime anywhere near to this; rather P_D would be expected to be many orders of magnitude higher than P_F for any system which is to see real use. Therefore, it is likely less computationally time intensive to provide a reasonable estimate of the $\mathcal{H}_1$ CDF than it would be for values of interest under $\mathcal{H}_1$. However, in multistatic passive radar applications, the system performance can be extremely sensitive to the SNR across the M channels, thus necessitating a large number of Monte Carlo simulations to account for variable operating conditions.

The following figure represents an example of a "half-analytical" ROC curve. More precisely, this figure shows an example in which the expressions for the $\mathcal{H}_0$ distribution of λ_1 given by (3.7) is used to compute thresholds for set values of probability of false alarm as previously seen in Section 4.1.2, while the corresponding probabilities of detection are computed using a Monte Carlo simulation of 10^3 trials. Unlike in the $\mathcal{H}_0$ case where the region of interest of the distribution includes extremely small probabilities of false alarm, it is of interest to have probabilities of detection on the order of 0.5 or greater. Thus, the relatively small Monte Carlo simulation provides an acceptable level of fidelity in this example.

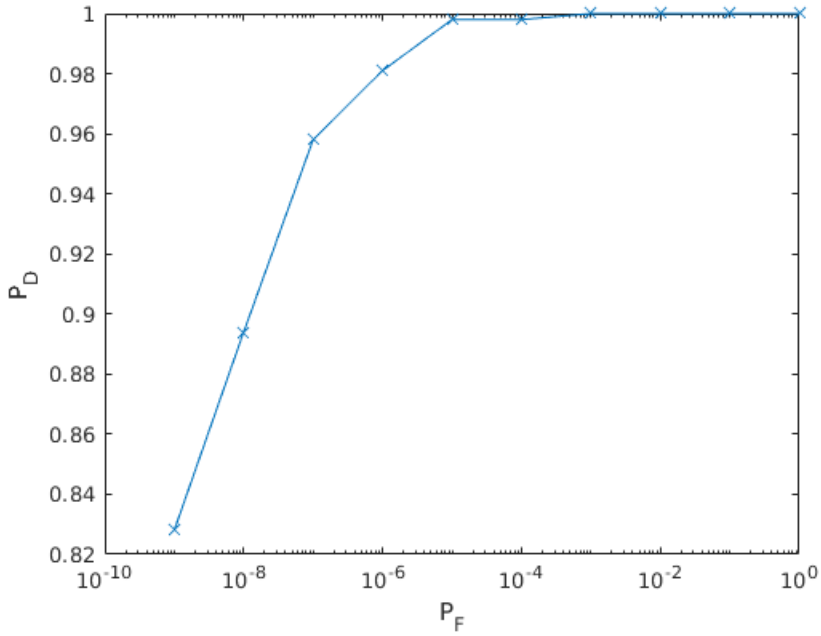

Figure 4.11: ROC Curve for $M = 4$, $N = 10^5$ with -22 dB per Channel SNR.

4.2 $\mathcal{H}_1$ Numerics

In this section, the method for computing the non-central CDF of λ_1 using (3.15) as presented in Section 3.2 is compared for small values of N with (2.17), and for larger values of N where floating point overflow problems surface against an empirical estimate of the CDF generated through Monte Carlo simulation. First, Section 4.2.1 discusses some numerical limitations with the result from the derivation in Section 3.2. Section 4.2.2 focuses on the direct computation of the CDF with the various outlined methods. The expressions for $F_{\lambda_1}^{\mathcal{H}_0}(x)$ and $F_{\lambda_1}^{\mathcal{H}_1}(x)$ are then combined to compute a receiver operating characteristic curve in closed form in Section 4.2.3.

4.2.1 Limitations Computing the Hypergeometric Function

Computing the distribution of λ_1 requires computation of values of the hypergeometric function ${}_0F_1(a+1, \mu_1(a+t\sqrt{2a}))$ during the numerical integration necessary to

find the values of the matrix elements in (3.15), over the interval $(-\sqrt{a/2}, y)$, where based on the substitutions demonstrated in Chapter 3 y is approximately in the range $(-5, 10)$. Recall ${}_0F_1$ is defined to be

$$ {}_0F_1(b, z) = \sum_{k=0}^{\infty} \frac{z^k}{(b)_k k!} \tag{4.1} $$

such that $(b)_k$ is the Pochhammer symbol or rising factorial. In many cases of a and μ_1 that are of interest in this problem, similar to the problems encountered throughout this dissertation with the gamma function, ${}_0F_1$ can overflow floating point representations. Numerical methods for computing ${}_0F_1$ in the particular regimes of interest has not seen particular interest in the literature, with methods primarily focusing on the confluent and Gaussian hypergeometric functions [32]. To overcome this limitation, note that the ${}_0F_1$ term in the integral appears in the first column of the matrices in both the numerator and denominator that normalizes the expression for the CDF given by (3.15). Therefore, as the determinant is a multilinear operator in the columns of the matrices, it is possible to multiply the first column in both numerator and denominator by some constant to in some sense normalize the hypergeometric function. As a proposed normalization constant, take μ_1^l for some integer value l. Next, expand ${}_0F_1$ with the particular arguments of interest multiplied by this constant, and computing each individual term in the summation in log space results in the following.

$$
\begin{aligned}
&\frac{1}{\mu_1^l}{}_0F_1(a+1,\mu_1(a+t\sqrt{2a})) \\
&\qquad = \frac{1}{\mu_1^l}\sum_{k=0}^{\infty}\frac{\mu_1^k(a+t\sqrt{2a})^k}{(a+1)_k k!} \\
&\qquad = \sum_{k=0}^{\infty}\exp\left(\log\left(\frac{\mu_1^k(a+t\sqrt{2a})^k}{(a+1)_k k!}\right)\right) \\
&\qquad = \sum_{k=0}^{\infty}\exp\Big((k-l)\log\mu_1 + k\log(a+t\sqrt{2a}) \\
&\qquad + \log\Gamma(k+1) + \log\Gamma(a+1) - \log\Gamma(a+1+k)\Big)
\end{aligned}
$$

Note that the $\log\Gamma$ terms can be computed using Stirling's formula. By adjusting the parameter l it is possible to compute values of this hypergeometric function in many cases that are of interest for the multi-channel detection problems discussed throughout this dissertation, though this approach is not particularly sophisticated and will still suffer from numerical overflow in extremely large cases that could be of interest in some applications.

4.2.2 CDF Comparison

Consider first the small problem comparing (2.17) and (3.15), the original gamma function like form of the non-central distribution and the D polynomial formula derived in Section 3.2. Fig. 4.12 plots these two CDFs.

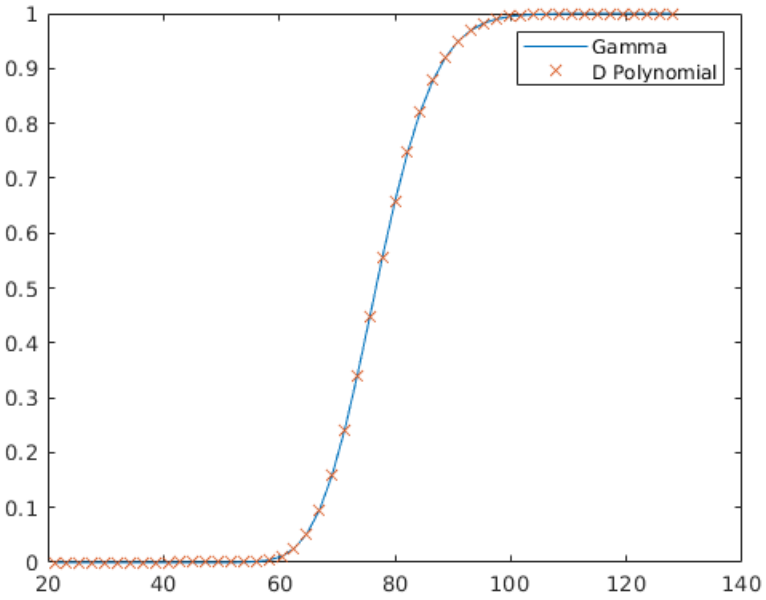

Figure 4.12: Comparison of $F_{\lambda_1}^{\mathcal{H}_1}(x)$ Calculated Using (2.17) and (3.13), (3.14) for $M = 2$ and $N = 64$ with -5 dB per Channel SNR.

Note the absolute mean-squared error between the two methods is on the order of machine epsilon.

Next, consider a larger problem, which must be addressed with Monte Carlo methods as (2.17) overflows double precision floating point arithmetic for values of N larger than those shown in Table 2.3. Fig. 4.13 compares the CDF computed using (3.15) and an empirical CDF generated through Monte Carlo simulations.

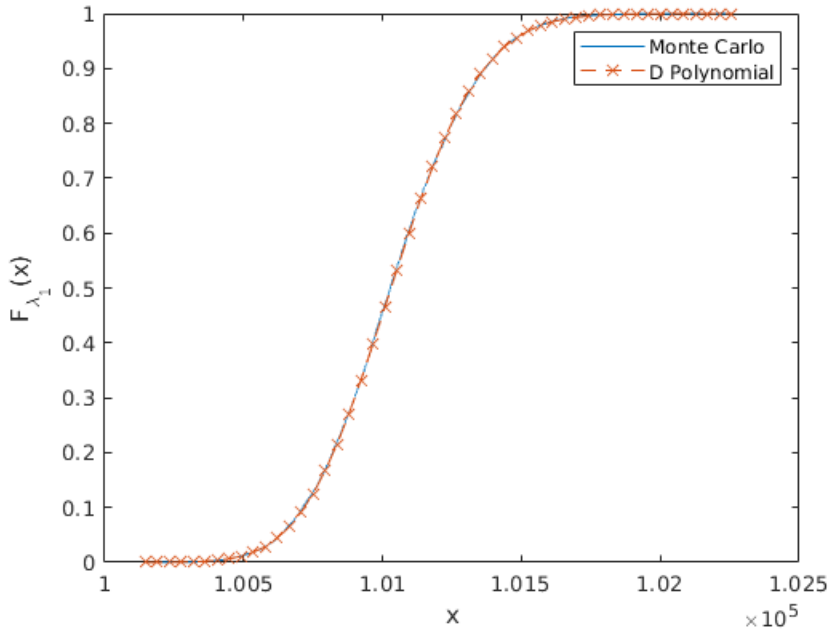

Figure 4.13: Comparison of $F_{\lambda_1}^{\mathcal{H}_1}(x)$ Calculated Using (3.15) and a Monte Carlo Simulation with 10^6 Trials for $M = 4$ and $N = 10^5$ with -28 dB per Channel SNR.

4.2.3 Receiver Operating Characteristic

In a passive radar application, the primary goal of computationally tractable formulas for the distribution of the GLRT statistic under both the $\mathcal{H}_0$ and $\mathcal{H}_1$ hypotheses is to compute exactly the probability of false alarm $P_F = 1 - F_{\lambda_1}^{\mathcal{H}_1}(T)$ and the probability of detection $P_D = 1 - F_{\lambda_1}^{\mathcal{H}_1}(T)$. The threshold value T is generally set to maintain a constant P_F as required for a particular system's operation. Previously, the $\mathcal{H}_1$ case could only be approached via Monte Carlo simulation; the expression (3.15) allows P_D to be computed to arbitrary precision.

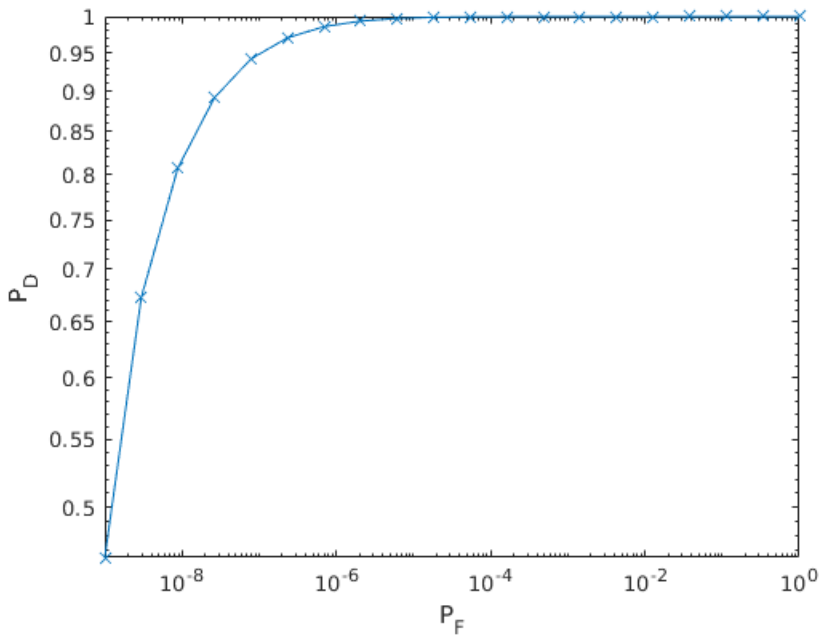

Figure 4.14: P_F vs P_D Computed Using Exact Expressions for $F_{\lambda_1}(x)$ Calculated Using (3.15) and a Monte Carlo Simulation with 10^6 Trials for $M = 4$ and $N = 10^4$ with -15 dB per Channel SNR.

Note that due to the overflow problems with the hypergeometric function discussed in Section 4.2.1, the methods discussed throughout this dissertation may not be sufficient to fully characterize all cases of interest under the $\mathcal{H}_1$ signal model, primarily in cases where the SNR is relatively high for large values of N.

4.3 Monte Carlo Methods

This section will discuss computing (false alarm) event probabilities for the largest eigenvalue of (central) Wishart matrices, i.e., $P_F = P(\lambda_1 > x)$ through Monte Carlo simulation. Of particular interest are cases in which x is relatively large, leading the small probabilities of false alarm on the order of 10^{-8} to 10^{-12}, so-called rare events. In particular, Monte Carlo simulation and methods to reduce the variance of resulting estimates and thus the computational overhead of such simulations are

of interest in cases that are intractable analytically (large degrees of freedom) or in which well known (TW) approximations fail [23]. For completeness, naive Monte Carlo simulation methods will be examined, though it is obvious that the number of samples required for fidelity using these methods will not be practical for the values of P_F that are of interest. Subsequently, the current state of the art for importance sampling techniques are discussed.

4.3.1 Naive Monte Carlo Simulations and the Bartlett Decomposition

The Wishart distribution is often thought of as the distribution of the $M \times M$ Gramian constructed from an $M \times N$ Gaussian matrix, i.e.,

$$W = X^{\dagger}X$$

Thus it is apparent that the first method of generating random samples of the largest eigenvalue λ_1 of W can be computed by finding the square of largest singular value of an $M \times N$ matrix of random Gaussian draws.

$$\lambda_1 = \max\left(\mathrm{SVD}(X)^2\right)$$

In remote sensing applications, M is generally small (< 10), but N may be on the order of 10^6 or larger. Clearly, generating millions of independent Gaussians for every trial and then computing the M singular values for this large matrix is computationally intensive. Thus, the second method for generating samples of λ_1, the Bartlett decomposition, involves generating only the $M \times M$ Wishart matrix itself and subsequently computing the eigenvalues of this matrix [33]. The Bartlett decomposition of a (complex) Wishart matrix is a Cholesky factorization

$$W = AA^{\dagger}$$

where A is a lower triangular matrix of with elements

$$A = \begin{pmatrix} c_1 & 0 & 0 & \cdots & 0 \\ n_{21} & c_2 & 0 & \cdots & 0 \\ n_{31} & n_{32} & c_3 & \cdots & 0 \\ \vdots & \vdots & \vdots & \ddots & \vdots \\ n_{M1} & n_{M2} & n_{M3} & \cdots & c_M \end{pmatrix}.$$

The elements of A are random variables with distributions $c_i \sim \sqrt{\Gamma(N-M+i,1)}$ and $n_{i,j} \sim \mathcal{CN}(0,1)$ [34]. Then a single sample of λ_1 can be computed as

$$\lambda_1 = \max\left(\text{eig}\left(AA^\dagger\right)\right).$$

Using this Bartlett decomposition approach requires the generation of M Gamma distributed random samples and $M(M-1)/2$ standard complex Gaussians. Given that there are various fast numerical algorithms for generating Γ samples, this is a significant improvement when N is large. However, in cases where one may be interested in computing $P_F = P(\lambda_1 > x)$ for a value of x where, for example, P_F is on the order of 10^{-9}, it is still necessary to generate an enormous number of these Bartlett decomposition matrices to have any hope of an accurate probability estimate. Note a Bartlett decomposition may also be derived in the non-central case. For a rank K non-centrality, the matrix is reduced to a block format consisting of a $M-K \times M-K$ central Wishart (which can be computed using the above Bartlett decomposition) and $K \times K$ non-central Wishart along the diagonal, with a $M-K \times K$ standard complex normal matrix and its conjugate transpose filling in the remainder of the matrix [35].

4.3.2 Introduction to Importance Sampling

Importance sampling is a technique in which a random sample is drawn from one distribution and transformed through some functional relationship into a sample

from another distribution of interest. The distribution of interest may be intractable to sample from for a variety of reasons, including intractable analytic expressions or computing the probability of a rare event, from which the name derives. If the probability density function of the distribution of interest is f and it is desired to compute some integral $I = E_f[h(X)]$, sample random variables with distribution corresponding to density g, as

$$\begin{aligned} I &= E_f[h(X)] \\ &\int h(x)f(x)dx \\ &= \int \frac{h(x)f(x)}{g(x)} g(x)dx \\ &= E_g\left[\frac{h(x)f(x)}{g(x)}\right]. \end{aligned}$$

For rare event simulation, h is often the indicator function of (T, ∞). Then the key to performance of this technique is the choice of the distribution g. The optimal distribution, in the sense that it minimizes the variance of the importance sampling estimator, is

$$g^*(x) = \frac{|h(x)|\, f(x)}{E_f\left[h(X)\right]}.$$

This does not give insight into a method to actually find such g^*, which may require significant careful analysis. This is beyond the scope of this dissertation.

4.3.3 Importance Sampling Algorithm for λ_1

The current state of the art for importance sampling for the largest eigenvalue distribution of Wishart matrices derives from Jiang et al. [24]. The algorithm proposed to compute the probability $P(\lambda_1 < Nx)$ generates samples of the ordered eigenvalues $\lambda_1 > \ldots > \lambda_M$ and then computes an importance samping estimator. The proposed algorithm is as follows.

Step 1: *Generate a matrix* $L_{M-1,N-1,\beta} = B_{M-1,N-1,\beta}B^T_{M-1,N-1,\beta}$ *where* B *is an* $M-1 \times M-1$ *bidiagonal matrix defined as*

$$B_{M-1,N-1,\beta} = \begin{pmatrix} \chi_{\beta(N-1)} & & & 0 \\ \chi_{\beta(M-2)} & \chi_{\beta(N-2)} & & \\ & \ddots & \ddots & \\ 0 & & \chi_{\beta} & \chi_{\beta(N-(M-1))} \end{pmatrix}.$$

Step 2: *Conditional on* $\lambda_2, \ldots, \lambda_M$ *sample* λ_1 *from the exponential distribution.*

$$f(\lambda_1) = \frac{x-\beta}{2x} e^{-\frac{x-\beta}{2x}(\lambda_1 - \max(Nx,\lambda_2))} \cdot I_{\lambda_1 > \max(Nx,\lambda_2)}$$

Step 3: *Compute the estimator* L_N.

$$L_N = \frac{MA_M \prod_{i=2}^{M} (\lambda_1 - \lambda_i)^{\beta} \lambda_1^{\frac{\beta(N-M+1)}{2}-1} e^{-\frac{\lambda_1}{2}}}{\frac{x-\beta}{2x} e^{-\frac{x-\beta}{2x}} I_{\lambda_1 > \max(Nx,\lambda_2)}} I_{\lambda_1 > Nx}$$

In these expressions I is the indicator function. Note that $\beta = 1, 2, 4$ corresponding to the real, complex, and quaternion cases, respectively. This process is repeated P times, and the estimate for the probability $P(\lambda_1 > Nx)$ is the mean of the samples $L_N^{(i)}$.

$$P(\lambda_1 > Nx) \approx \frac{1}{P} \sum_{i=1}^{P} L_N^{(i)}$$

4.3.4 Importance Sampling Performance Analysis

In applications to remote sensing (multi channel radar) or MIMO communications, the data derives from physical signals which are modeled as complex valued samples. Note that consequently in Step 2 of the algorithm the exponential pdf is not well defined for values of x less than $\beta = 2$.

The following is presented not as a formal argument, but to provide mathematical intuition as to why this importance sampling algorithm loses efficacy in regimes of interest to multi channel sensing. As $N, M \to \infty$ at a fixed ratio ($N/M \to c$) the probability that all eigenvalues lies within the Marčenko-Pastur support of

$$\left[(\sqrt{N} - \sqrt{M})^2, (\sqrt{N} + \sqrt{M})^2\right]$$

approaches 0.9397 [36]. In the problems of interest for multi channel sensing, where N is large and M is small, it may be intuitively thought of that the distribution curve is "narrowing" relative to the value of N. The values of x used in the importance sampling algorithm corresponding to $T = N \times x$ for computing probabilities of false alarm $P_F = \int_T^\infty f$ are slightly over 1 for probabilities of false alarm of interest (i.e., $\approx 10^{-9}$). As mentioned in the previous paragraph, this is not well defined in the exponential distribution sampling step of the importance sampling algorithm.

Although analysis is not tractable for the cases of interest for remote sensing, with complex data and large values of N, analysis of importance sampling for rare events for relatively small N and M is feasible using this method. Sample R code supplied by the authors of [24] can be found at [37].

In a small test case, parameters of $M = 2$, $N = 64$ were used and the importance sampling algorithm was performed with 10^3 and 10^5 trials.

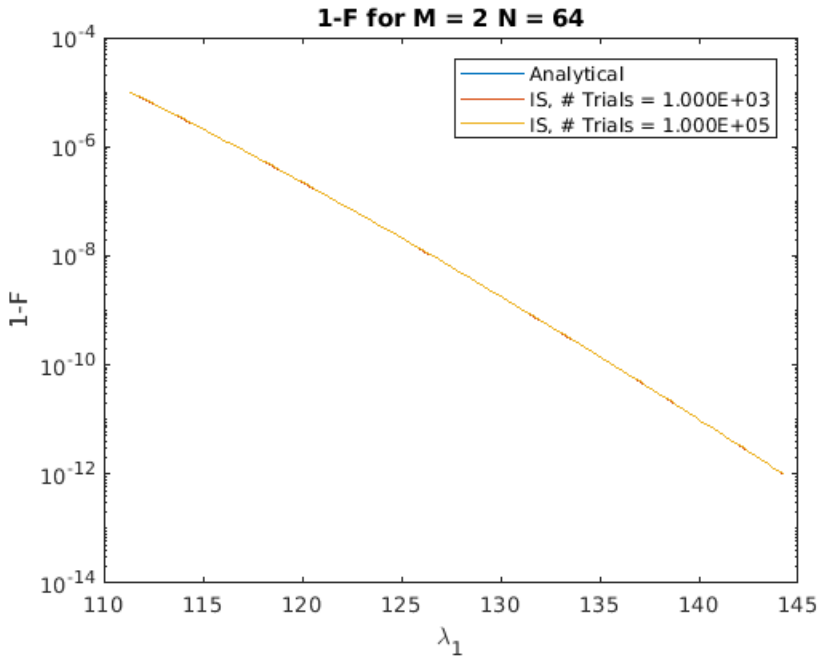

Figure 4.15: Importance Sampling and Analytical Complementary CDFs.

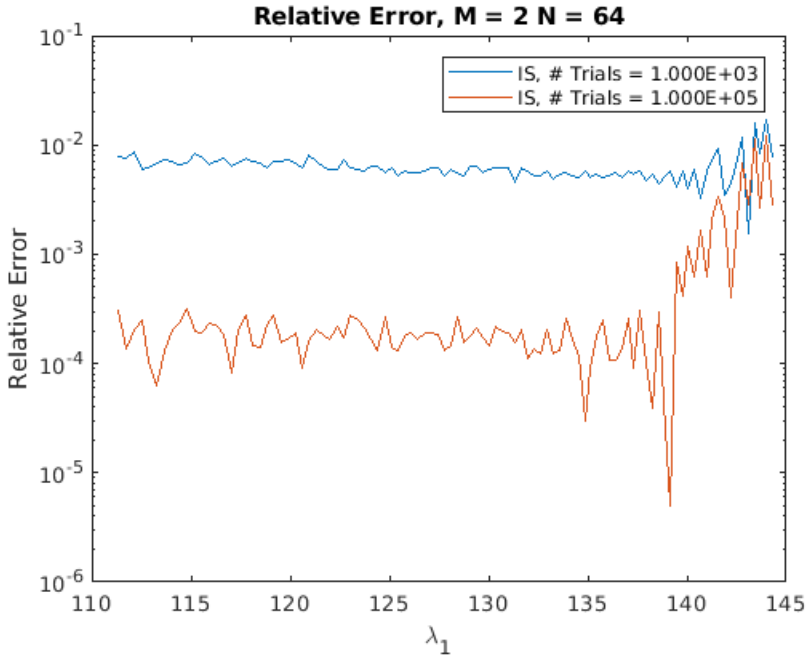

Figure 4.16: Relative Error from Analytical to Importance Sampling Calculations of Complementary CDFs.

It is apparent that the relative error improves by running the importance sampling algorithm with 10^5 trials as opposed to with 10^3. However, there also appears to be a threshold at which the relative error increases significantly, corresponding to the true probability decreasing in magnitude and causing an increase in the variance of the importance sampling estimate. This corresponds to findings by the authors of this method; the expected value of the error between the importance sampling estimate and either naive Monte Carlo or the analytical formulation is approximated as a function of the number of trials and the magnitude of the complementary CDF at a given point [24].

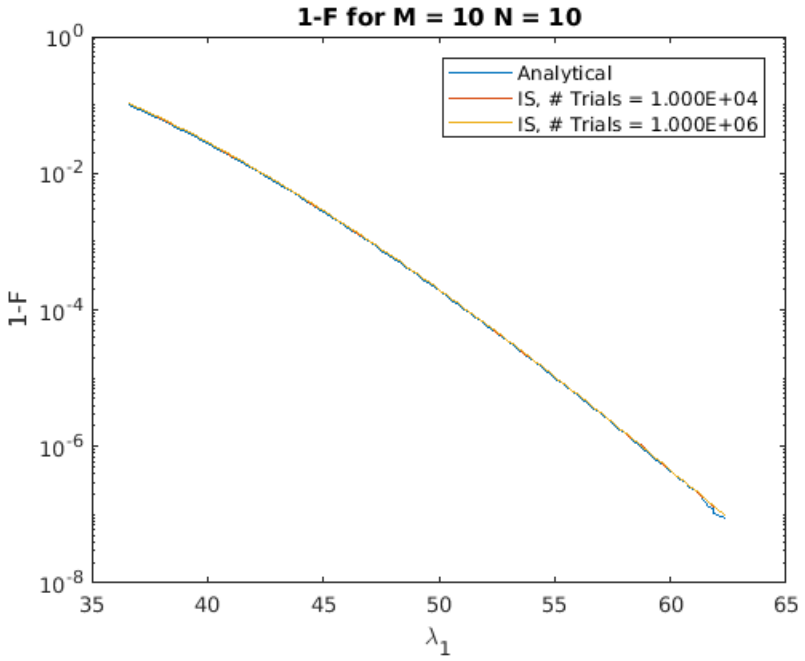

Figure 4.17: Importance Sampling and Analytical Complementary CDFs.

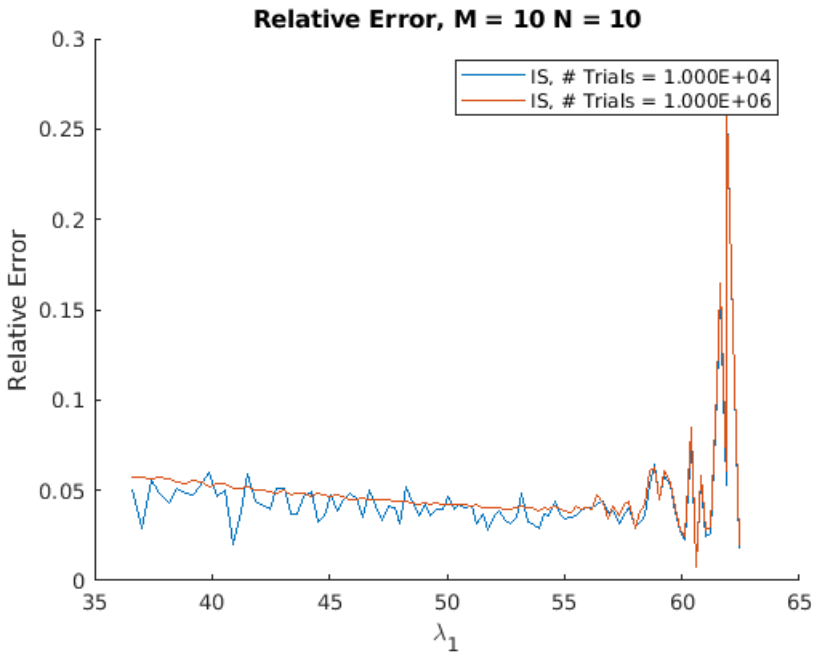

Figure 4.18: Relative Error from Analytical to Importance Sampling Calculations of Complementary CDFs.

Although the problem of calculating $P(\lambda_1 < Nx)$ is not as evident in this example problem, the relative error is significantly worse in the smaller sized, "square" experiment, even with an order of magnitude higher number of trials as compared to the previous test. As previously discussed, the importance sampling method that is detailed throughout this paper is designed by taking a limit in N and M at a fixed ratio, and as such is not well tailored to this problem.

The importance sampling method demonstrated in this section is currently considered the state of the art for a less computational intensive Monte Carlo estimator for the largest eigenvalue of Wishart matrices. There are obvious limitations, namely that it was primarily designed with the real case in mind, and has severe limitations in the complex case when $N \gg M$. However, it should be noted that this method is by no means unique nor guaranteed to be optimal. With careful analysis it would likely be possible to design a distribution from which to sample that would be well tailored

to importance sampling for the particular problem cases of interest for multi-channel sensing. In addition, it is likely possible to utilize alternative Monte Carlo variance reduction techniques, or methods such as large deviations to estimate probabilities far in the tail of the largest eigenvalue distribution.

4.3.5 Monte Carlo Timing Analysis

This section presents some analysis on the expected time required to compute probabilities using the various methods of Monte Carlo simulation, and compares them to the computational cost of computing values of the CDF of λ_1 using an exact expression as derived and shown in Section 3.1.

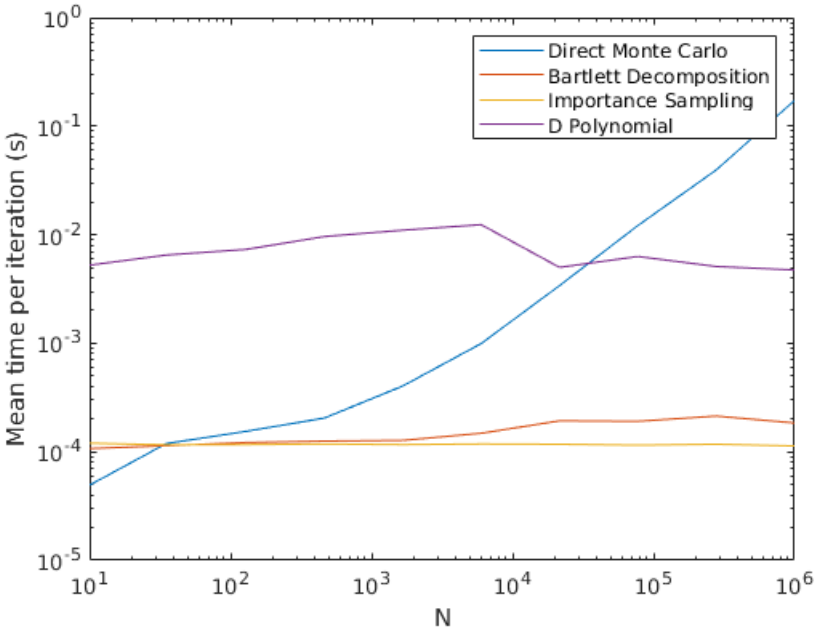

Figure 4.19: Computation Time to Generate One Sample of λ_1 Using Naive Monte Carlo, Bartlett Decomposition, Importance Sampling, or to Compute the Value of the CDF Directly at One Point Using Exact Expression Given by (3.7). All Experimental Results are for $M = 4$.

Fig. 4.19 demonstrates the amount of CPU time necessary to compute one pseudo random draw from the distribution of λ_1 using the direct Monte Carlo, Bartlett De-

composition, and Importance Sampling methods described earlier in this section. Note that the importance sampling draws are not meaningful in computing probabilities as they fall outside the algorithm domain as detailed in Section 4.3.2; however the results are illustrative in terms of the computation time required.

The first key takeaway from Fig. 4.19 is that clearly a direct Monte Carlo simulation is not a feasible option for computing probabilities in the central Wishart cases, where probabilities of false alarm typically encountered are often on the order of 10^{-9}. This means even for small values of N the computational costs are at least seven orders of magnitude higher than using the closed form D-polynomial expression for the distribution to compute just one point in the tail of the distribution. Even if it was of interest to tabulate a large number of points in the distribution, direct Monte Carlo simulation is extremely time intensive compared to direct computation, especially as the memory requirements start to climb for larger values of N.

Note that the Bartlett Decomposition, Importance Sampling, and exact D polynomial timing results are much less dependent on N than direct Monte Carlo simulation. Each of these methods takes N as a parameter to the problem, but computation is performed using matrices of size $M \times M$ for the Bartlett Decomposition and D polynomial methods and $(M-1) \times (M-1)$ for the Importance Sampling algorithm, considerably lessening the inherent memory overhead. For very small values of N, approximately less than 100, these methods perform worse than direct Monte Carlo due to additional overhead in the software, but are clearly a major improvement in regimes of interest to these problems. However, as it is of interest to compute values of the complementary CDF corresponding to probabilities of false alarm on the order of 10^{-9}, large numbers of trials are still required. Using the Bartlett decomposition, this means that computing a single point of the CDF with any accuracy requires at least seven orders of magnitude more computation than a single point using the

exact D polynomial expression. Recall that the purpose of importance sampling is to transform fewer samples from some distribution to estimate some function that would require drawing more samples from some other distribution. Some theoretical bounds are given in [24] regarding the number of trials required, albeit experimental validation is required to demonstrate values of the constants in these expressions to determine the number of trials to run. In general, it seems gaining two to three orders of magnitude versus other Monte Carlo methods is reasonable. This still results in the Importance Sampling algorithm being at least five orders of magnitude more time consuming than computing using an exact expression, to say nothing of the fact that the algorithm fails to produce meaningful results in cases of interest for multistatic passive radar in which N is large and M is small.

4.4 Detection Simulation

This section presents a simulation of an ambiguity function generated in a multistatic passive radar scenario. The formulas for the probability distributions of λ_1 presented in the previous sections are used to compute detection thresholds in this simulated scenario. Results from a particular example are given as a demonstration of the utility of the distributions derived in earlier sections for performing multistatic detection.

4.4.1 Test Parameters

Consider the signal model presented in Section 2.1. This was simulated in MATLAB with a single stationary transmitter and M stationary receivers. The simulated scatterer was assumed to be stationary, or equivalently, the results shown examine the zero Doppler slice for Doppler corrected data. Various illuminating waveforms and other RF system parameters such as transmit power, noise temperature, receiver

beam pattern, etc. were set to realistic values for fixed commercial transmitters, radar receivers, and realistic scatterers. The M receivers were modeled as having a narrow scanning beam recording N samples for each position in a surveyed two dimensional grid. Complex white Gaussian noise was added to the received data at a power level corresponding to the signal bandwidth and a receiver operating at room temperature. It is assumed the direct path copy of the transmitted signal is eliminated from the receivers through a very deep null in beamforming or through environmental obstruction, such that the received data contains only noise or copies of the transmitted signal that have reflected off the target.

4.4.2 Detection Results

Each receiver was simulated as scanning the two dimensional grid in the area of interest, recording N samples from the simulated environment, and performing the data alignment described in Section 2.1. Subsequently, a Gram matrix $X^\dagger X$ was formed from the data recorded at each of the M receivers, and $\lambda_1(X^\dagger X)$ calculated to perform detection. Detection thresholds were set using the D-polynomial expression for the distribution of λ_1 under the null hypothesis $\mathcal{H}_0$ as given by (3.7). Consider the simulated system geometry. In this simulated environment, each of the M receivers collected N samples which were passed to a fusion center, corrected for the hypothesized position in order to compute λ_1 to decide on the presence of a target with the given hypothesized state.

First, consider illumination of a target with a circularly symmetric complex Gaussian waveform. In practice, generating a Gaussian illumination signal would be extremely difficult. However, in a Gaussian communications channel with a power constraint, a Gaussian sequence with the variance determined by this power constraint maximizes the mutual information and thus the channel capacity [38]. In this

example, a transmitter with an omnidirectional antenna emits a Gaussian signal at a specified power level. Each of the M receivers scans the specified grid in the (X, Y) plane with a narrow antenna beam and records N samples. If the beam is steered towards the target, these samples will contain copies of the transmitted signal scattered off the target that has been delayed, Doppler shifted, and with a corresponding power loss due to spherical propagation, as given by the radar range equation [39].

$$P_M = P_T \frac{\sigma G_T G_M \lambda^2}{(4\pi)^3 R_T^2 R_M^2} \tag{4.2}$$

Here P_M is the power at receiver M, P_T the transmitted power, G_T and G_M the antenna gains of the transmitter and receiver M, σ the radar cross section of the scatterer, and R_T and R_M the propagation path lengths between the transmitter and scatterer and the scatterer and receiver M. In the case where the target is an emitter, the electromagnetic propagation is not bistatic and the R_T term may be eliminated from the equation.

If the beam is not steered towards the target, no scattered waveform will be recorded and the receiver data will contain only white Gaussian noise. The data at each receiver is time and Doppler aligned according to the posited physical state of the target whose presence is to be ascertained, and the largest eigenvalue λ_1 of the Gram matrix $X^\dagger X$ formed from this corrected data is calculated. Consider the following simulated geometry. In this scenario, $M = 2$ receivers each collect $N = 10^4$ samples for each postulated target position on a discretized grid of the area under surveillance. Each receiver has equal noise power and recorded data will contain independent zero mean complex white Gaussian noise. Recorded data may contain the transmitted signal scattered off the target, with appropriate delays and channel gains corresponding to the path length between the transmitter, target, and receiver, and the antenna gain corresponding to the beamforming performed at each receiver

based on the putative target position currently under test. It is assumed there is a null in this beam pattern in the direction of the transmitter.

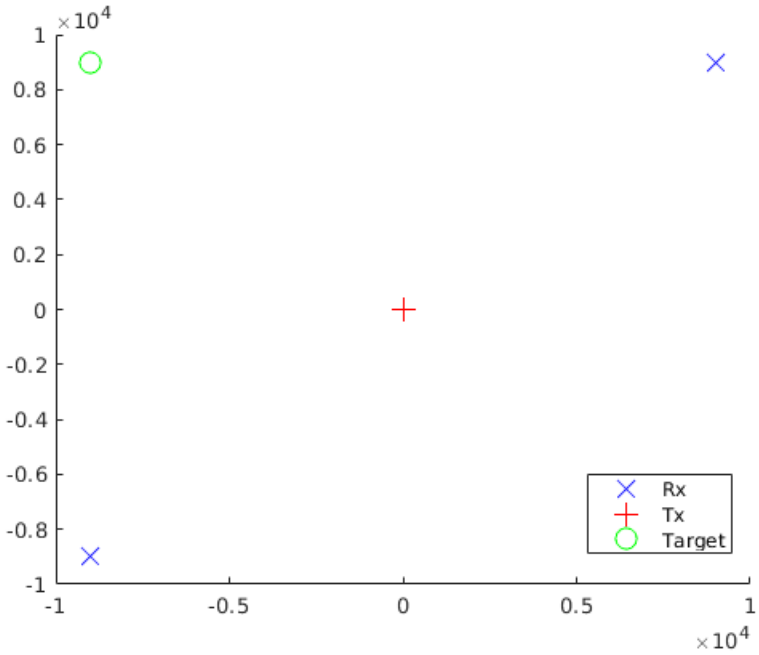

Figure 4.20: Simulated Geometry of Two Receivers, One Transmitter, and One Target.

The approximate SNR at each receiver for data collected corresponding to the true target position is -7.3 dB. In this example, the target is assumed to be stationary. Using the expressions for the distributions under $\mathcal{H}_0$ and $\mathcal{H}_1$ given by (3.7) and (3.15), the expected ROC for this scenario can be seen in Fig. 4.21.

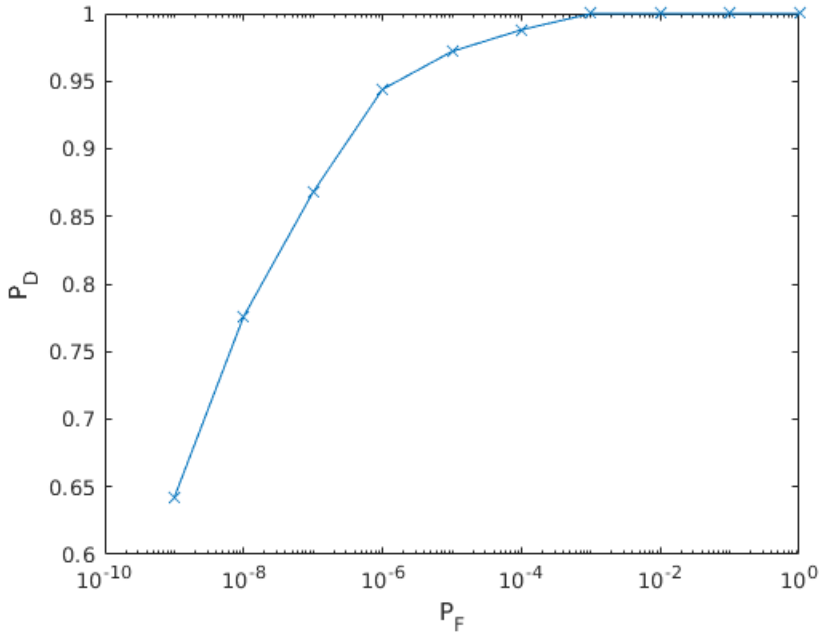

Figure 4.21: Expected ROC for Simulation Scenario.

Calculating the detection statistic λ_1, it is possible to produce an image corresponding to the problem geometry that is analogous to the zero-Doppler slice of the Woodward ambiguity function. Consider the following, with the value of λ_1 corresponding to each position on the (X, Y) grid, with the data corrected for the time delay corresponding to this position.

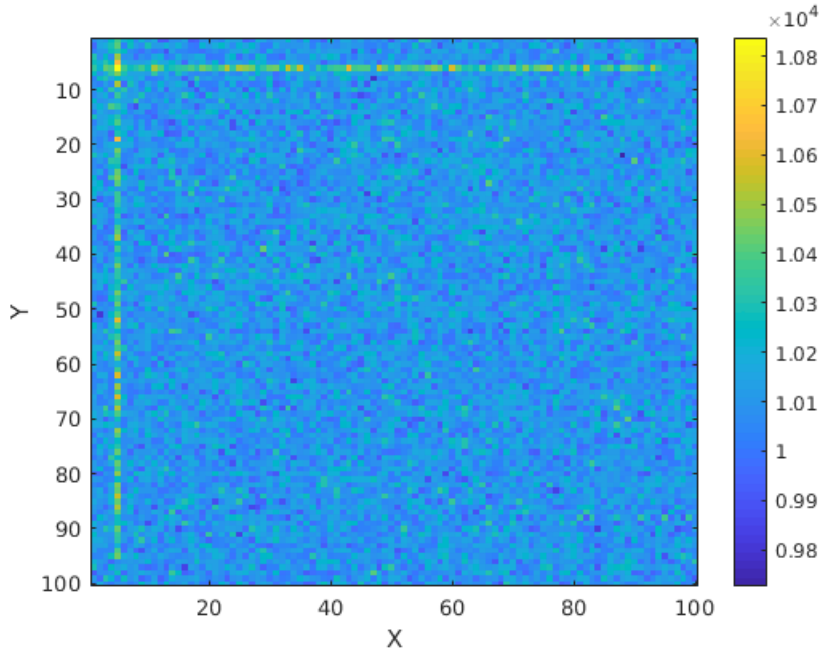

Figure 4.22: Grid of the Detection Statistic λ_1 for Corrected Data Corresponding to Each Hypothesized Physical Location of the Target with Gaussian Illumination.

Note that clearly there is a bright spot corresponding to the true target location. However, it is also important to note that for some hypothesized positions, the data recorded at each receiver does not exactly correspond to either the $\mathcal{H}_0$ or $\mathcal{H}_1$ hypotheses. The stripes between the true target location and receivers correspond to some signal scattered off the target being recorded on one receiver. The received data in this scenario results in a non-central Wishart distribution for the Gram matrix, but with only one non-zero column in the mean. If a detection threshold is set too low, the entirety of this region could result in a false detection. The probability of false alarm is set to relatively small values to avoid this. Consider the following map of detections performed on the previously shown ambiguity function, with threshold values computed for a particular probability of false alarm using (3.7).

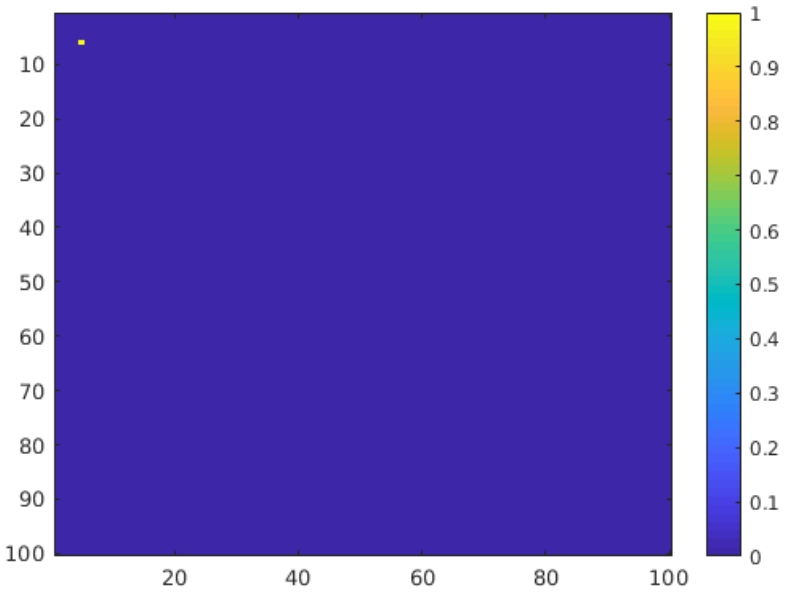

Figure 4.23: Detections Resulting from the Values of λ_1 Shown in Fig. 4.22 Using a Threshold Corresponding to a $P_F = 10^{-7}$ with Gaussian Illumination.

Using a defined acceptable probability of false alarm to set an appropriate detection threshold for this problem calculated using (3.7), the D polynomial distribution under the null hypothesis, a decision can be made to determine if the value of λ_1 in each cell on this grid corresponds to hypothesis $\mathcal{H}_0$ or $\mathcal{H}_1$. In this example, with $P_F = 10^{-7}$ the striping seen in Fig. 4.22 caused by scattered signal energy recorded at each receiver for hypothesized positions in the direct path of the target does not result in false detections.

Next, consider a more realistic example of illumination by a truncated linear chirp waveform, which may actually be used in a radar system. Consider the same geometry as shown in Fig. 4.20, again with $N = 10^4$ samples, $M = 2$ transmitters, and setting simulation parameters such that for signals scattered from the true target location result in a per channel SNR of -7.3 dB. The system should again perform per the ROC curve given by Fig. 4.21. As before, consider the test statistic λ_1 for each

position in the (X, Y) grid.

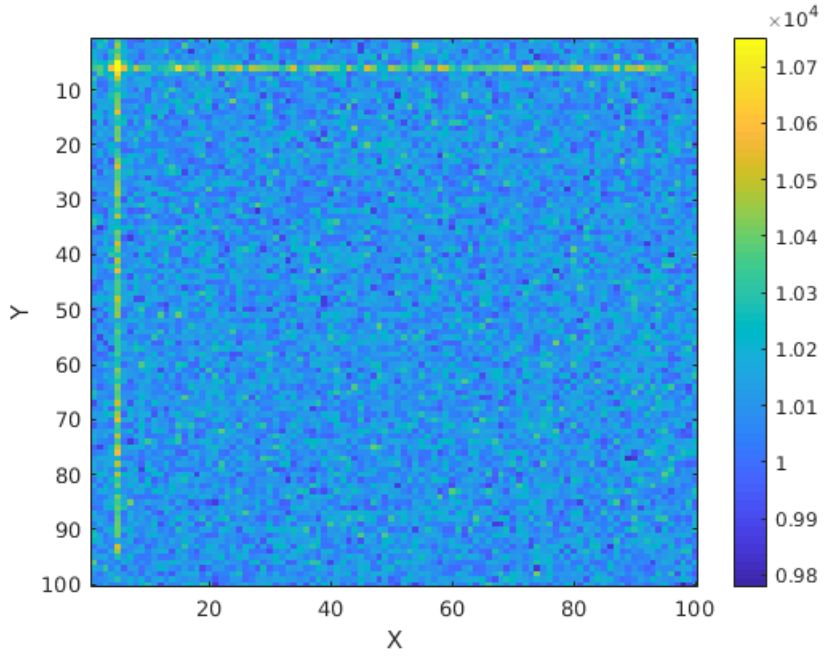

Figure 4.24: Grid of the Detection Statistic λ_1 for Corrected Data Corresponding to Each Hypothesized Physical Location of the Target with Linear Chirp Illumination.

It is clear that there is a bright spot corresponding to the target, but that it is slightly more spread around the true scatterer location. This is due to the fact that the autocorrelation of the truncated chirp is not as narrow around the peak as that of the Gaussian illumination signal. This increased correlation causes slightly misaligned copies of the signal to still produce higher values of the detection statistic λ_1 than seen in the Gaussian case. Again, take $P_F = 10^{-7}$, and consider the following map of detections.

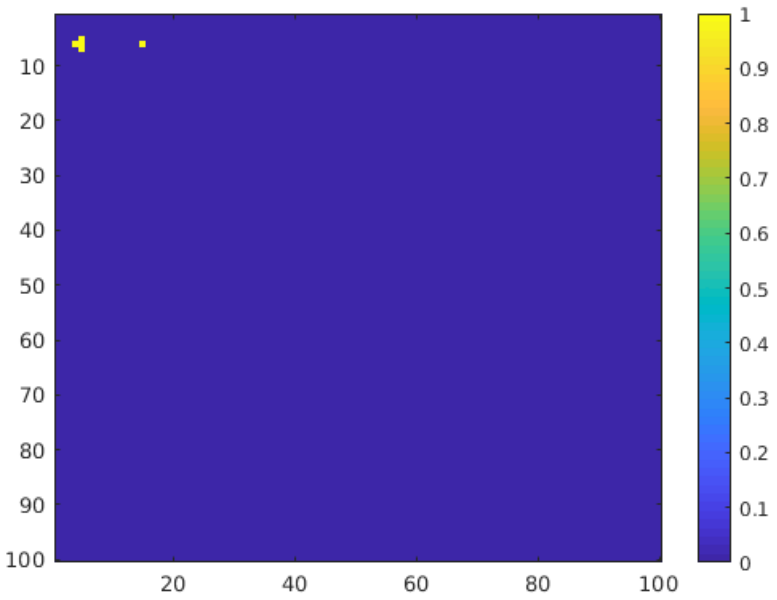

Figure 4.25: Detections Resulting from the Values of λ_1 Shown in Fig. 4.22 Using a Threshold Corresponding to a $P_F = 10^{-7}$ with Linear Chirp Illumination.

Note that as may be anticipated by the autocorrelation properties of the illumination signal, there are detections in the cells adjacent to the true target location. Note also that there is an ambiguous detection several cells further away. The signal is only present on one of the channels when this cell is under test, which corresponds to neither the $\mathcal{H}_0$ nor $\mathcal{H}_1$ hypotheses discussed for most of this dissertation. This highlights the need for additional signal processing or a human operator to help to distinguish which of several adjacent cells actually contains the target, or cause the system to throw out ambiguous detections. This process can be aided by additional information or assumptions, such as an understanding of the illumination waveform ambiguity properties or other physical properties of the system or environment.

Chapter 5

CONCLUSION

This chapter aims to summarize the results presented in previous chapters of this thesis and present future directions for research in this area and with related problems. First, a variety of possible extensions to this problem are presented in Section 5.1. Extensions of the methods used to compute probability distributions from the largest eigenvalue to functions of several eigenvalues of a complex Wishart matrix, as well as some discussion of a geometric interpretation of the problem present the primary proposed theoretical extensions of the work. Further discussion is given to the possibility of extending existing work on Monte Carlo methods, engineering concerns that could arise when attempting to implement these results as part of a detection algorithm on a real physical system, and on applications to related problems in the fields of detection, estimation, and random matrix theory. Section 5.2 summarizes the contents of this thesis and outlines the specific contributions that have been presented.

5.1 Future Work

The work presented in this thesis is a theoretical derivation of computationally tractable expressions for the CDF of λ_1, the largest eigenvalue of a complex Wishart matrix, with a stated intent of applying these results to compute probabilities of false alarm and detection to characterize multi-channel detection performance in passive radar. Tractable formulas for the distributions are presented that allow for computation of probabilities in both the central and non-central Wishart cases, corresponding to the null and alternative hypotheses in the multistatic passive radar detection problem model presented as motivation.

These results represent significant contributions to the current state of the art, but there are many directions in which this work could be extended. First and foremost, it would be ideal to be able to have closed form, computationally tractable expressions for the distribution of the GLRT statistic for rank K detection, which is the rank K partial trace of the Gram matrix formed from collected data. This represents a formidable problem in which some progress has been made, but presents significant challenges and opportunity to extend this work. In addition to considering the application of methods similar to those seen throughout this thesis, it has been proposed to approach this problem through a very general geometric presentation of the joint distribution of the eigenvalues of a complex Wishart matrix. From a theoretical perspective, examining these distributions from the most general geometric perspective is in itself is a worthwhile direction of future work. Although this work is motivated by a desire to avoid empirical characterization of a distribution via Monte Carlo simulation, that area represents an area in which significant progress is also possible. There are also a number of further practical engineering concerns that would arise in implementation of a detection algorithm utilizing these distributions on a real system, including illumination waveform performance, communications bandwidth limitations, and scenarios in which the received data does not completely fit either the null or alternative hypothesis leading to ambiguities. Finally, the theory that has been presented has applications to other problems both in remote sensing and in related areas such as MIMO communications, as well as to random matrix theory. Various related problems could possibly benefit from the approaches detailed in this thesis or perhaps provide insight into extensions of this work.

5.1.1 Higher Rank Detection

The GLRT and Bayesian test statistics for a common rank-K component in the mean across M receivers were shown to be functions of the partial and complete trace of the Gram matrix constructed from data, dependent on if the noise power is known or unknown, by Sirianunpiboon et al. [20]. In the most general case in which K is unknown, the GLRT is the determinant of the Gram matrix, which is known to have a distribution that is a product of independent Beta variates [40]. In the case that the rank of the signal of interest is equal to (or greater than) the number of sensors, GLRT is the trace of the Gram matrix. In this case, the distribution can be computed using the Bartlett decomposition of a central Wishart matrix. This section discusses the more general case of this problem, where the rank of the common component in the mean is $K < M$, and examines the complications of integrating the joint PDF of the ordered eigenvalues of a complex Wishart matrix over the polytope defined by the partial trace. Some computation for the particular case of rank $K = 2$ detection with $M = 3$ is presented as an example.

First, the joint PDF of the ordered eigenvalues of W is given by

$$f(\lambda_1, \ldots, \lambda_M) = ce^{-\sum_{i=1}^{M} \lambda_i} \prod_{i=1}^{M} \lambda_i^{N-M} \prod_{j=1}^{M-1} \prod_{k=j+1}^{M} (\lambda_j - \lambda_k)^2 \tag{5.1}$$

where c is a normalization constant [11].

To determine the distribution of the statistic (i.e. if one wishes to compute thresholds), $\lambda_{k+1}, \ldots, \lambda_m$ must be marginalized out of the distribution given by (5.1), at which point the resultant joint PDF of $\lambda_1, \ldots, \lambda_k$ can be integrated over the region

$$\mathcal{D}_x = \{x \geq \lambda_1 \geq \ldots \geq \lambda_M \geq 0\} \cap \left\{ x \geq \sum_{i=1}^{K} \lambda_i \geq 0 \right\}. \tag{5.2}$$

To find the CDF for some value of x. Pictorially, for the $K = 2$ case this corresponds to integrating over the region show in Fig. 5.1.

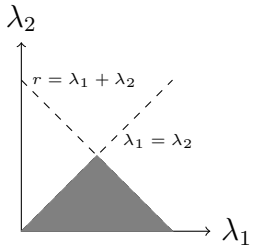

Figure 5.1: Integration Region for the First Two Largest Eigenvalues

As an example, in the case $K = 2$, $M = 3$, this corresponds to the integral

$$\left[\int_0^{x/2}\int_0^{\lambda_1}\int_0^{\lambda_2} + \int_{x/2}^{x}\int_0^{x-\lambda_1}\int_0^{\lambda_2}\right] f(\lambda_1, \ldots, \lambda_M) d\lambda_3 d\lambda_2 d\lambda_1. \tag{5.3}$$

This case is fairly simple to write, and can be generalized for arbitrary K and M to fit the appropriate polytope as defined by (5.2). However, computing the integral presents some difficulties. First, consider marginalizing out the variables $\lambda_{K+1}, \ldots, \lambda_M$. Expanding the quadratic terms of the joint PDF given by (5.1) will result in a polynomial with terms of the generic form

$$a \prod_{i=1}^{M} e^{-\lambda_i} \lambda_i^{l_i}$$

where leading constant a and exponents l_i arise from expanding the polynomial terms of the PDF. Computing the marginalization integral of λ_M results in these terms becoming

$$\int_0^{\lambda_{M-1}} a \prod_{i=1}^{M} e^{-\lambda_i} \lambda_i^{l_i} d\lambda_M = a\gamma(l_M, \lambda_{M-1}) \prod_{i=1}^{M-1} e^{-\lambda_i} \lambda_i^{l_i} \tag{5.4}$$

where $\gamma(n, x)$ is the lower incomplete gamma function. Note that, it can be shown that γ satisfies the recurrence relation

$$\gamma(n+1, x) = n\gamma(n, x) - x^n e^{-x}.$$

Applying the recurrence relation multiple times it is apparent

$$\begin{aligned}\gamma(n,x) &= (n-1)\gamma(n-1,x) - x^{n-1}e^{-x} \\ &= (n-1)\left((n-2)\gamma(n-2,x) - x^{n-2}e^{-x}\right) - x^{n-1}e^{-x} \\ &\cdots\end{aligned}$$

Following the recurrence n times and noting that $\gamma(0,x) = 1$ results in the identity

$$\gamma(n,x) = (n-1)!\left(1 - e^{-x}\sum_{k=0}^{n-1}\frac{x^k}{k!}\right). \tag{5.5}$$

Substituting the formula for the incomplete gamma function given in (5.5) into (5.4) results in

$$\begin{aligned}&a\gamma(l_M,\lambda_{M-1})\prod_{i=1}^{M-1}e^{-\lambda_i}\lambda_i^{l_i} \\ &= a(l_M-1)!\left(1 - e^{-\lambda_{M-1}}\sum_{k=0}^{l_M-1}\frac{\lambda_{M-1}^k}{k!}\right)\prod_{i=1}^{M-1}e^{-\lambda_i}\lambda_i^{l_i} \\ &= a(l_M-1)!\left(e^{-\lambda_{M-1}}\lambda_{M-1}^{l_{M-1}} - e^{-2\lambda_{M-1}}\sum_{k=0}^{l_M-1}\frac{\lambda_{M-1}^{l_{M-1}+k}}{k!}\right)\prod_{i=1}^{M-2}e^{-\lambda_i}\lambda_i^{l_i}.\end{aligned}$$

It is then possible to compute the integral of terms of this form in the same manner as previously to marginalize out λ_{M-1}, and iterate upon this process to marginalize out the eigenvalues of index greater than K.

After marginalizing the low order eigenvalues, it is then of interest to compute the integral of the joint PDF over the polytope defined by the summation term given in (5.2). Note that in the example case of $K = 2$, $M = 3$, the integral is split into two pieces. The first, $\int_0^{x/2}\int_0^{\lambda_1} d\lambda_2 d\lambda_1$ can be approached using the same summation expansion as in the marginalization integrals. The second, $\int_{x/2}^{x}\int_0^{x-\lambda_1} d\lambda_2 d\lambda_1$, can also be expanded using the recurrence identity (5.5) and the first integral computed, resulting in terms of the form

$$\int_{x/2}^{x} \alpha e^{-\lambda_1} \lambda_1^{l_1} \left(1 - e^{-(x-\lambda_1)} \sum_{k=0}^{l_1} \frac{(x-\lambda_1)^{k+l_2}}{k!}\right) d\lambda_1$$

where α contains multiplicative constants and lower order terms. Factoring the leading $e^{-\lambda_1}\lambda_1^{l_1}$ through results in

$$\int_{x/2}^{x} \alpha \left(e^{-\lambda_1} \lambda_1^{l_1} - e^{-x} \sum_{k=0}^{l_1} \frac{\lambda_1^{l_1}(x-\lambda_1)^{k+l_2}}{k!}\right) d\lambda_1.$$

The first term of the summation is, as before, an incomplete gamma function. Changing variables with the substitution $u = \lambda_1/x$ the second term takes the form of the upper incomplete beta function, which is defined as

$$B(x; a, b) = \int_x^1 t^a (1-t)^b dt.$$

Combining these incomplete beta function pieces with the gamma function pieces, the final version of the distribution takes the general form

$$\begin{aligned} F_{\sum_{i=1}^{K} \lambda_i}(x) = &\sum_i a_i \sum_{k=0}^{l_i} \frac{\gamma(l_i, x)}{2^{l_i} k!} \\ &+ \sum_j b_j \sum_{k=0}^{m_j} \frac{x^{m_j+k}}{k!} B\left(1/2; m_j, k\right) \\ &+ \sum_k c_k \gamma(n_k, x). \end{aligned} \tag{5.6}$$

Where a_i, b_j, c_k are constants and l_i, m_j, n_k are integers of approximately order $N - M$ to $N + M$ that arise through the polynomial expansion. Exact expressions for particular cases can be computed by explicitly expanding the joint PDF of the order eigenvalues given by (5.1). However, using these expressions to compute probabilities is not practical. As a CDF the range of this function is $[0, 1]$. In addition to the extremely large gamma function terms that have been a major focus throughout this work, there is significant subtractive cancellation occurring which is extremely numerically unstable.

It is likely that an alternative approach must be taken to achieve significant progress in a computationally tractable methodology for computing the distribution of the partial trace of a complex Wishart matrix. It may be that it is possible to work directly with the joint PDF of the ordered eigenvalues to find an expression that is amenable to computation via numerical integration. There is also a push to understand the geometric connection between the generalized Laguerre polynomials and the distribution of Wishart eigenvalues, which may yield an approach allowing integration of (5.1) over any arbitrary region of its support.

5.1.2 Monte Carlo Simulation

It is natural to consider the approach of characterizing the distribution of λ_1 empirically through Monte Carlo simulation. While this may be feasible for small problems, naive Monte Carlo is not suited to multistatic passive radar applications. This is primarily a consequence of the memory requirements for problems in which N is large and the long computation time required to generate sufficient pseudo-random trials to be statistically meaningful in the tails of the distribution. There exists some work on variance reduction techniques, primarily importance sampling, in which it is of interest to compute some quantity $E_f\left[h(X)\right]$ where X has density f, by noting that

$$E_f\left[h(X)\right] = E_g\left[\frac{h(X)f(X)}{g(X)}\right]$$

for some other distribution g. Samples are then drawn from g, which can then be transformed to compute the quantity of interest. The performance gains (i.e., the number of pseudo random trials that must be generated for accurate probabilities) are generally fairly modest. In addition, finding a suitable g may be very non-trivial. Results exists on importance sampling for a particular class of this problem, taking a limit in N, M at a fixed ratio, but it is of limited use in this multi-channel sensing

problem. For further discussion of the current state of this research direction, see Section 4.3.2.

5.1.3 Engineering Concerns

The results presented here are concerned primarily concerned with using a closed form expression for the distribution of the GLRT to compute ROC curves, but from an engineering perspective this does not fully characterize system performance. Some results on ambiguity performance in realistic passive radar scenarios exist [7], and a basic simulation is presented in this work in Section 4.4. However, this is certainly not exhaustive nor representative of all the additional engineering challenges that would be faced in deploying these techniques as part of the detection algorithm on a real system. This problem is highly motivated by a passive radar scenario in which one does not control the waveform, therefore analysis of ambiguity properties of common waveforms deployed on illuminators of opportunity in the environment (i.e., communications signals) in a multistatic case would be very valuable. Although difficult to carry out in a general research context, it is highly important to understand further system specific limitations to truly characterize detection performance, such as the the effects of clutter or limitations and non-linearities induced by RF hardware .

The presented results on the distributions of λ_1 under both $\mathcal{H}_0$ and $\mathcal{H}_1$ are sufficient to characterize system performance for arbitrary N, but practically speaking, the choice of numerical integration algorithm and consequent limits on the number of integration intervals or increased computation time may limit the size of N. It is also clearly the case that beyond a certain problem size, verification via Monte Carlo is infeasible due to physical memory limitations and computation time constraints. It is also apparent that, particularly in the $\mathcal{H}_1$ case it is possible that the formulas for the distribution may return infinite or NaN values when given an argument outside

the domain; care must be taken in numerical implementations to avoid this.

5.1.4 Other Related Problems

There are many related problems motivated by multistatic detection in which distributions of some functions of the spectrum of a Gram matrix constructed from data arise. One variation of the problem that has generated significant interest is the case in which data vector at each receiver has been normalized to unit length. Normalizing null-hypothesis data consisting of white Gaussian noise results in vectors uniformly distributed on the unit sphere. Generalized Coherence provides a well studied approach to detection for normalized data [5]. Similar techniques to those used by Cochran et al. to factor the Gram matrix and compute the distribution of its determinant has potential application in computing the distribution of the trace of complex Wishart matrices, as discussed in the second problem.

In addition to expansions of the work as motivated by multi-channel passive radar systems, there is potential to apply similar techniques to other multi-channel problems. There has also been a renewed interest in work pioneered by Gardener in the 1990's in detecting cyclostationary signals through properties of the autocorrelation, or applying known detection results for single cycle detection [41] [42]. Recent work by Ramirez et al. develops a detector that is a function of the determinant of block diagonal representations of covariance matrices [43]. These detectors are all functions of the spectrum of the data covariance, and as such may admit the application of similar techniques to the problems examined in this research. In many cases, the $\mathcal{H}_0$ model in these problems is the same as that used throughout this dissertation. However, concerns about sensitivity of these problems to a sampling rate commensurate with the period of the cyclic autocorrelation of cyclostationary signals has been noted; careful analysis must be performed if this is to be pursued.

5.2 Summary

This thesis presents new methods for tractable numerical computation of the distribution of the largest eigenvalue of a complex Wishart matrix in various cases. Motivation for this problem comes from detection of a rank-one signal in the mean of additive white Gaussian noise across multiple receivers in a multistatic passive radar system. In the binary hypothesis problem that arises from the signal model in this problem, the largest eigenvalue of the Gram matrix constructed from the data has a complex Wishart distribution, and the largest eigenvalue λ_1 of this matrix is the GLRT. It is thus of interest to compute probabilities of the distribution of λ_1 in the signal absent case in which only noise is present across each of the receivers, as well as under the signal present case in which a common rank-one signal is present in the mean. The problem is formulated and a signal model developed in Section 2.1. Classical results on the distribution of λ_1 are presented in 2.4, and the numerical limitations and a discussion of the why these results are unsuitable for use in the problem of interest was presented in 2.5.

The primary novel contributions of this thesis are computationally tractable formulas for the distribution of λ_1 under both the signal absent (central Wishart) and signal present (non-central Wishart) cases. Explicit formulas for both of these distributions are well known and documented in the literature, they are unsuitable for computation in regimes of interest due to very large gamma function terms. Although as a probability distribution the final value must be in $[0, 1]$, the known expressions rely on cancellation via ratios of these extremely large gamma function terms, which overwhelm double precision floating point representations. This work discusses the connection between the gamma function and the generalized Laguerre polynomials, and demonstrates an expansion of the distribution formulas in both the central and

non-central cases as inner products of these orthogonal polynomials. Further analysis is performed to eliminate numerical overflows through leading constants and additional gamma function like terms, eventually resulting in equations that can be used to compute probabilities in cases with large degrees of freedom using numerical quadrature. These results may be seen in Section 3.1 for the central case, and Section 3.2 for the non-central case. Although not directly related to the motivating problem of multistatic passive radar detection, the presented techniques can also be applied to the case of a central correlated Wishart matrix, in which the covariance matrix is arbitrary. For completeness, these results are presented in 3.3. A survey of Monte Carlo methods for approximating these distributions is given in Section 4.3 along with a discussion of their limitations and shortcomings in cases of interest.

Numerical results presented in this thesis are motivated primarily by the multistatic passive radar problem in which it is desirable to characterize detection performance using these distributions. The central and non-central formulas derived in the theoretical portion of this thesis are compared to previously known closed form expressions in small cases and to empirical distributions constructed from Monte Carlo trials in cases that would overwhelm these closed form expressions from the literature. Using the central distribution formula, detection thresholds based on a chosen acceptable probability of false alarm are computed, and the corresponding probability of detection was computed in closed form using the non-central distribution. Using these results, fully analytical receiver operating characteristic are generated. Chapter 4 presents these results, beginning with a comparison of methods of computing probabilities, and subsequently using the results from Sections 3.1 and 3.2 to compute detection thresholds and receiver operating characteristic curves. A simulation of a multistatic passive radar detection scenario is shown in 4.4, in which the theoretical results are used to set thresholds and perform detection on simulated data in a realis-

tic scenario. Certain practical engineering concerns are noted, including a discussion of the limitations of the signal model and the necessity to take this into account when implementing these theoretical detection results as a portion of an algorithm on a real system.

Possible future extensions to this work are presented in Section 5.1. Expanding this work to be able to compute the distribution of a rank-K partial trace of a complex Wishart matrix would be the ideal generalization. This section gives some preliminary derivations and further discussions on why this is a very difficult problem to approach directly, as well as some discussion on geometric insights that may prove a useful tool in working towards this generalization. In addition, some further discussion of related research directions in detection and estimation using tools from random matrix theory is discussed.

REFERENCES

[1] M. Kang and M. S. Alouini, "Largest eigenvalue of complex Wishart matrices and performance analysis of MIMO MRC systems," *IEEE Journal on Selected Areas in Communications*, vol. 21, no. 3, pp. 418–426, April 2003.

[2] K. S. Bialkowski and I. V. L. Clarkson, "Computing multistatic passive radar CFAR thresholds from surveillance-only data," in *Proceedings of the IEEE International Conference on Acoustics, Speech and Signal Processing*, April 2015, pp. 5555–5559.

[3] S. Jin, M. R. McKay, X. Gao, and I. B. Collings, "MIMO multichannel beamforming: SER and outage using new eigenvalue distributions of complex noncentral Wishart matrices," *IEEE Transactions on Communications*, vol. 56, no. 3, pp. 424–434, March 2008.

[4] I. M. Johnstone, Z. Ma, P. O. Perry, and M. Shahram, "RMTstat: Distributions, statistics and tests derived from random matrix theory," Nov 2014. [Online]. Available: https://CRAN.R-project.org/package=RMTstat

[5] D. Cochran, H. Gish, and D. Sinno, "A geometric approach to multiple-channel signal detection," *IEEE Transactions on Signal Processing*, vol. 43, no. 9, pp. 2049–2057, 1995.

[6] A. Leshem and A.-J. van der Veen, "Multichannel detection of Gaussian signals with uncalibrated receivers," *IEEE Signal Processing Letters*, vol. 8, no. 4, pp. 120–122, 2001.

[7] K. S. Bialkowski, I. V. L. Clarkson, and S. D. Howard, "Generalized canonical correlation for passive multistatic radar detection," in *Proceedings of the IEEE Signal Processing Workshop*, July 2011, pp. 417–421.

[8] D. Ramírez, G. Vazquez-Vilar, R. López-Valcarce, J. Vía, and I. Santamaría, "Detection of rank-P signals in cognitive radio networks with uncalibrated multiple antennas," *IEEE Transactions on Signal Processing*, vol. 59, no. 8, pp. 3764–3775, 2011.

[9] D. E. Hack, L. K. Patton, and B. Himed, "Multichannel detection of an unknown rank-one signal with uncalibrated receivers," in *Proceedings of the IEEE International Conference on Acoustics, Speech, and Signal Processing*, May 2014, pp. 2987–2991.

[10] D. E. Hack, C. W. Rossler, and L. K. Patton, "Multichannel detection of an unknown rank-N signal using uncalibrated receivers," *IEEE Signal Processing Letters*, vol. 21, no. 8, pp. 998–1002, 2014.

[11] A. M. Tulino and S. Verdú, *Random Matrix Theory and Wireless Communications*, ser. Foundations and Trends in Communications and Information Theory, 2004, vol. 1, no. 1.

[12] T. Ratnarajah, "Complex singular Wishart matrices and multiple-antenna systems," in *IEEE/SP 13th Workshop on Statistical Signal Processing, 2005*, July 2005, pp. 1032–1037.

[13] A. Kortun, M. Sellathurai, T. Ratnarajah, and C. Zhong, "Distribution of the ratio of the largest eigenvalue to the trace of complex Wishart matrices," *IEEE Transactions on Signal Processing*, vol. 60, no. 10, pp. 5527–5532, October 2012.

[14] N. R. Goodman, "Statistical analysis based on a certain multivariate complex Gaussian distribution (an introduction)," *Annals of Mathematical Statistics*, vol. 34, no. 1, pp. 152–177, 1963.

[15] C. G. Khatri, "Distribution of the largest or the smallest characteristic root under null hypothesis concerning complex multivariate normal populations," *Annals of Mathematical Statistics*, vol. 35, no. 4, pp. 1807–1810, Dec 1964.

[16] P. Graczyk, G. Letac, and H. Massam, "The complex Wishart distribution and the symmetric group," *Annals of Statistics*, vol. 31, no. 1, pp. 287–309, 2003.

[17] D. E. Hack, L. K. Patton, B. Himed, and M. A. Saville, "Centralized passive MIMO radar detection without direct-path reference signals," *IEEE Transactions on Signal Processing*, vol. 62, no. 11, pp. 3013–3023, June 2014.

[18] A. Clausen and D. Cochran, "An invariance property of the generalized coherence estimate," *IEEE Transactions on Signal Processing*, vol. 45, no. 4, pp. 1065–1067, 1997.

[19] K. Beaudet and D. Cochran, "Multiple-channel detection in active sensing," in *Proceedings of the IEEE International Conference on Acoustics, Speech, and Signal Processing*, May 2013, pp. 3910–3914.

[20] S. Sirianunpiboon, S. D. Howard, and D. Cochran, "Multiple-channel detection of signals having known rank," in *2013 IEEE International Conference on Acoustics, Speech and Signal Processing*, May 2013, pp. 6536–6540.

[21] M. Chiani, M. Z. Win, and A. Zanella, "On the capacity of spatially correlated MIMO Rayleigh-fading channels," *IEEE Transactions on Information Theory*, vol. 49, no. 10, pp. 2363–2371, Oct 2003.

[22] C. A. Tracy and H. Widom, "Level-spacing distributions and the Airy kernel," *Physics Letters B*, vol. 305, no. 1-2, pp. 115–118, 1993.

[23] S. N. Majumdar and M. Vergassola, "Large deviations of the maximum eigenvalue for Wishart and Gaussian random matrices," *Physical Review Letters*, vol. 102, no. 6, p. 060601, Feb. 2009.

[24] T. Jiang, K. Leder, and G. Xu, "Rare-event analysis for extremal eigenvalues of white Wishart matrices," *ArXiv e-prints*, Aug. 2014.

[25] K. Beaudet and D. Cochran, "Estimation of subspace occupancy," in *2014 48th Asilomar Conference on Signals, Systems and Computers*, Nov 2014, pp. 1599–1603.

[26] S. Jones, S. Howard, I. Clarkson, K. Bialkowski, and D. Cochran, "Computing the largest eigenvalue distribution for complex Wishart matrices," in *Proceedings of the IEEE International Conference on Acoustics, Speech, and Signal Processing*, March 2017.

[27] N. M. Temme, *Special Functions: An Introduction to the Classical Functions of Mathematical Physics*. Wiley, 1996.

[28] S. Jones, D. Cochran, S. Howard, I. Clarkson, and K. Bialkowski, "Computing the largest eigenvalue distribution for non-central Wishart matrices," in *Proceedings of the IEEE International Conference on Acoustics, Speech, and Signal Processing*, May 2019.

[29] T. W. Anderson, "The non-central Wishart distribution and certain problems of multivariate statistics," *Ann. Math. Statist.*, vol. 17, no. 4, pp. 409–431, 12 1946. [Online]. Available: http://dx.doi.org/10.1214/aoms/1177730882

[30] G. Alfano, A. Lozano, A. M. Tulino, and S. Verdú, "Mutual information and eigenvalue distribution of MIMO Ricean channels," *Proc. of ISITA 2004*, pp. 10–13, 2004.

[31] P. Dharmawansa and M. R. McKay, "Extreme eigenvalue distributions of some complex correlated non-central Wishart and gamma-Wishart random matrices," *ArXiv e-prints*, Jan. 2011.

[32] J. W. Pearson, S. Olver, and M. A. Porter, "Numerical methods for the computation of the confluent and gauss hypergeometric functions," *arXiv e-prints*, p. arXiv:1407.7786, Jul 2014.

[33] T. Anderson, *An Introduction to Multivariate Statistical Analysis*, ser. Wiley Series in Probability and Statistics. Wiley, 2003. [Online]. Available: https://books.google.com/books?id=Cmm9QgAACAAJ

[34] M. S. Bartlett, "XX. On the theory of statistical regression," *Proceedings of the Royal Society of Edinburgh*, vol. 53, pp. 260–283, 1934.

[35] D. G. Kabe, "A note on the Bartlett decomposition of a Wishart matrix," *Journal of the Royal Statistical Society. Series B (Methodological)*, vol. 26, no. 2, pp. 270–273, 1964. [Online]. Available: http://www.jstor.org/stable/2984422

[36] M. Chiani, "On the probability that all eigenvalues of Gaussian, Wishart, and double Wishart random matrices lie within an interval," *IEEE Transactions on Information Theory*, vol. 63, no. 7, pp. 4521–4531, July 2017.

[37] G. Xu, "Importance sampling estimator," 2014. [Online]. Available: http://users.stat.umn.edu/~xuxxx360/IS.R

[38] C. E. Shannon, "Communication in the presence of noise," *Proceedings of the IRE*, vol. 37, no. 1, pp. 10–21, Jan 1949.

[39] C. A. Balanis, *Antenna Theory: Analysis and Design*. New York, NY, USA: Wiley-Interscience, 2005.

[40] H. Gish and D. Cochran, "Generalized coherence." in *ICASSP, IEEE International Conference on Acoustics, Speech and Signal Processing - Proceedings*. IEEE, 1988, pp. 2745–2748.

[41] W. A. Gardner, "Exploitation of spectral redundancy in cyclostationary signals," *IEEE Signal Processing Magazine*, vol. 8, no. 2, pp. 14–36, April 1991.

[42] S. Enserink and D. Cochran, "On detection of cyclostationary signals," in *ICASSP, IEEE International Conference on Acoustics, Speech and Signal Processing - Proceedings*, vol. 3, 1995, pp. 2004–2007.

[43] D. Ramírez, P. J. Schreier, J. Vía, I. Santamaría, and L. L. Scharf, "Detection of multivariate cyclostationarity," *IEEE Transactions on Signal Processing*, vol. 63, no. 20, pp. 5395–5408, Oct 2015.

APPENDIX A

SOURCE CODE

A.1 Introduction

Included in this section is a description of MATLAB source code for computing the distribution of λ_1 using the closed form expressions under the various cases presented throughout this thesis, as well as ancillary code that is generally of interest to this problem. The code in question will be uploaded as a publically available github repository.

A.2 Wishart Matrix Tools

The following documented MATLAB scripts and functions are useful to compute the probability distribution of the largest eigenvalue λ_1 of a complex Wishart matrix under various cases of interest. In particular, these functions are designed for use in problems in which the size of the matrix $M \times M$ is reasonably small, while the degrees of freedom parameter N is quite large.

The included functions for computing the distribution of λ_1 follow the below naming convention:

[C, NC, S]_[CDF, CCDF]_[D, H, G, MC].m

Such that the abbreviations are as follows:

- [C, NC, S]: the type of complex Wishart matrix, (C)entral uncorrelated, (NC) non-central, or central correlated with (S)igma covariance.
- [CDF, CCDF]: computes the (CDF) or complementary CDF (CCDF), 1-CDF.
- [D,H,G,MC]: method of computing probabilities, (D) polynomials, (H)ermite polynomials, (G)amma functions, (MC) Monte Carlo.

Note that the included functions do not exhaust the combinatorics of the above.

C_CDF_D.m

Computes in closed form the central CDF of λ_1 using the D-polynomial formula given by (3.7).

- Arguments:
  - M: Size of the Wishart matrix
  - N: Degrees of freedom
  - x: Domain on which to compute values of the CDF.
- Returns:
  - F: CDF of λ_1

C_CDF_G.m

Computes in closed form the central CDF of λ_1 using Khatri's gamma function formula given by (2.15). Note that this formulation will overflow for approximately $N \geq 100$. For exact overflow points, see Table 2.1.

- Arguments:
  - M: Size of the Wishart matrix
  - N: Degrees of freedom
  - x: Domain on which to compute values of the CDF.
- Returns:
  - F: CDF of λ_1

C_CDF_H.m

Computes the central CDF of λ_1 using the Hermite polynomial formula given by (3.8). Note that this is asymptotic in N and thus most accurate for large values, but is computationally efficient as numerical quadrature integration is not required.

- Arguments:
  - M: Size of the Wishart matrix
  - N: Degrees of freedom
  - x: Domain on which to compute values of the CDF.
- Returns:
  - F: CDF of λ_1

C_CDF_MC.m

Generates an empirical CDF of λ_1 in the central case by generating pseudo-random complex Wishart matrices via a Bartlett decomposition as implemented in $wishrndC.m$.

- Arguments:
  - M: Size of the Wishart matrix
  - N: Degrees of freedom
  - $nTrials$: Number of pseudo-random trials to perform, length of returns F and x
- Returns:
  - F: CDF of λ_1
  - x: Support of the CDF F

C_CDF_IS.m

Generates an empirical CDF of λ_1 in the central case using the importance sampling algorithm discussed in [24].

- Arguments:
  - M: Size of the Wishart matrix.
  - N: Degrees of freedom.
  - x: Support of the CDF F.
  - $nTrials$: Number of pseudo-random trials to perform, length of returns F and x
- Returns:
  - F: CDF of λ_1

C_CCDF_D.m

Computes in closed form the central complementary CDF of λ_1 using the D-polynomial formula given by (3.7). Uses certain identities of the determinant to eliminate subtraction errors when computing $1 - F(x)$ when $F(x)$ is close to 1.

- Arguments:
  - M: Size of the Wishart matrix
  - N: Degrees of freedom
  - x: Domain on which to compute values of the CDF.
- Returns:
  - F: CDF of λ_1

C_CCDF_H.m

Computes asymptotically the central complementary CDF of λ_1 using the Hermite polynomial formula given by (3.7). Uses identities of the determinant to eliminate subtraction errors when computing $1 - F(x)$ when $F(x)$ is close to 1.

- Arguments:
  - M: Size of the Wishart matrix
  - N: Degrees of freedom
  - x: Domain on which to compute values of the CDF.
- Returns:
  - F: CDF of λ_1

NC_CDF_D.m

Computes in closed form the non-central CDF of λ_1 using the hypergeometric D-polynomial formula given by (3.15).

- Arguments:
  - M: Size of the Wishart matrix
  - N: Degrees of freedom
  - $mu1$: Dominant (only non-zero) eigenvalue of the non-centrality Gram matrix
  - x: Domain on which to compute values of the CDF.
- Returns:
  - F: CDF of λ_1

NC_CDF_G.m

Computes in closed form the non-central CDF of λ_1 using the hypergeometric gamma function formula given by (2.17).

- Arguments:
  - M: Size of the Wishart matrix
  - N: Degrees of freedom
  - $mu1$: Dominant (only non-zero) eigenvalue of the non-centrality Gram matrix
  - x: Domain on which to compute values of the CDF.
- Returns:
  - F: CDF of λ_1

NC_CDF_MC.m

Generates an empirical CDF of λ_1 in the non-central case by generating pseudo-random complex Wishart matrices via a direct Monte Carlo algorithm.

- Arguments:
  - M: Size of the Wishart matrix
  - N: Degrees of freedom
  - S: $M \times N$ signal in the mean. Assuming S is rank one, the largest eigenvalue of $S^{\dagger}S$ defines the SNR.
  - $nTrials$: Number of pseudo-random trials to perform, length of returns F and x

- Returns:
  - F: CDF of λ_1
  - x: Support of the CDF F

S_CDF_D.m

Computes in closed form the central correlated CDF of λ_1 using D-polynomial formula given by (3.25).

- Arguments:
  - M: Size of the Wishart matrix
  - N: Degrees of freedom
  - $sigma$: Length M vector of the eigenvalues of the covariance matrix of the Wishart matrix
  - x: Domain on which to compute values of the CDF.
- Returns:
  - F: CDF of λ_1

S_CDF_G.m

Computes in closed form the central correlated CDF of λ_1 using gamma function formula given by (2.18).

- Arguments:
  - M: Size of the Wishart matrix
  - N: Degrees of freedom
  - $sigma$: Length M vector of the eigenvalues of the covariance matrix of the Wishart matrix
  - x: Domain on which to compute values of the CDF.
- Returns:
  - F: CDF of λ_1

S_CDF_MC.m

Generates an empirical CDF of λ_1 in the central correlated case by generating pseudo-random complex Wishart matrices via a Bartlett decomposition as implemented in $wishrndC.m$.

- Arguments:

- M: Size of the Wishart matrix
- N: Degrees of freedom
- $Sigma$: $M \times M$ covariance matrix for the Wishart distribution
- $nTrials$: Number of pseudo-random trials to perform, length of returns F and x

- Returns:
  - F: CDF of λ_1
  - x: Support of the CDF F

wishrndC.m

Generates pseudo-random central complex Wishart matrices. For small values of N directly generates a matrix X and then computes the Wishart matrix $W = X^\dagger X$. For larger values of N, computes W directly using the Bartlett decomposition. These generated matrices be used to generate empirical CDF's of λ_1.

- Arguments:
  - $Sigma$: $M \times M$ covariance matrix, eye(M) for uncorrelated case, positive definite in general.
  - N: Degrees of freedom
  - D: Cholesky factorization of $Sigma$ - faster provided as argument if calling the function repeatedly.
  - n_trials: Number of matrixes to generate

- Returns:
  - W: $M \times M \times n\_trials$ array of Wishart matrices
  - D Cholesky factorization of $Sigma$

A.3 Multistatic Passive Radar Simulation

MATLAB code for the two dimensional multistatic passive radar simulation seen in section 4.4 is also made available. This code is designed to be general and modular, allowing arbitrary numbers of transmitters, receivers, and targets to be instantiated as arrays of objects containing the necessary data fields and functions to describe electromagnetic properties, and perform transmit, receive, and signal processing functions. The data generated in this simulation can be visualized as a plot of the geometry of the simulated problem, a spatial ambiguity function, and as a map of detections made using the thresholds computed using (3.7). The following gives a brief description of the structure and use of these tools.

Passive_sim.m

Master script that sets problem parameters and constructs Tx, Rx, Target, and FusionCenter objects. Calls methods from these functions to simulate the transmission, RF propagation, and receiving of data, as well as functions that perform signal processing to construct and plot system geometry, ambiguity functions, and detection outcomes.

Rx.m

Receiver object constructor. The number M receivers constructed defines the size of the Wishart distribution, the number of samples recorded at each receiver N is the degrees of freedom parameter in this distribution.

- Arguments:
  - param: Structure containing physical, RF, and signal processing parameters. Empty fields are automatically populated.
- External Functions:
  - ReceiveData: Collects data based on the location of the argument supplied Tx, Target, and hypothesized target position defining the direction in which the receiver antenna beam is pointed, including applying the appropriate delay and Doppler shifts if the received data has reflected off of a target.

Tx.m

Transmitter object constructor. Transmitted signal modes include frequency modulated audio (FM), random data frequency modulated (RAND), pure tone (SIN), QPSK, linear chirp (CHIRP), and Gaussian illumination (GAUSS).

- Arguments:
  - param: Structure containing physical, RF, and signal processing parameters. Empty fields are automatically populated.
- External Functions:
  - Transmit: Dependent on what transmit mode is selected, generates the transmitted signal and places into a buffer that can be accessed by the receiver.

Target.m

Target object constructor. Default behavior is to randomly generate a target with physical parameters that approximate a commercial airliner.

- Arguments:
  - param: Structure containing physical parameters. Empty fields are automatically populated.

FusionCenter.m

FusionCenter object constructor. Performs signal processing and target detection algorithms.

- Arguments:
  - param: Structure containing physical, RF, and signal processing parameters, as well as the Tx, Rx, and Target objects involved in the scenario. Empty fields are automatically populated.
- External Functions:
  - Ambiguity_XY: Calculates a two dimensional spatial ambiguity function, maximizing over the Doppler parameter.
  - Ambiguity_RD: Calculates a range-Doppler (Woodward) ambiguity function along a particular angle slice of the spatial domain, centered on coordinates $(0, 0)$. Defaults to the slice along which the target is located.
  - PlotAmbiguity: Creates an image of the ambiguity function calculated; labels axes as X,Y or Doppler, Range accordingly.